


# Exact moment analysis of transient/asymptotic dispersion properties in periodic media with adsorbing/desorbing walls

Cite as: Phys. Fluids **34**, 122013 (2022); <https://doi.org/10.1063/5.0130648>

Submitted: 13 October 2022 • Accepted: 30 November 2022 • Published Online: 19 December 2022

 Claudia Venditti,  Massimiliano Giona and  Alessandra Adrover



View Online



Export Citation



CrossMark



Physics of Fluids

Special Topic: Food Physics

Submit Today!

# Exact moment analysis of transient/asymptotic dispersion properties in periodic media with adsorbing/desorbing walls

Cite as: Phys. Fluids **34**, 122013 (2022); doi: 10.1063/5.0130648

Submitted: 13 October 2022 · Accepted: 30 November 2022 ·

Published Online: 19 December 2022



View Online



Export Citation



CrossMark

Claudia Venditti,<sup>a)</sup>  Massimiliano Giona,<sup>b)</sup>  and Alessandra Adrover<sup>c)</sup> 

## AFFILIATIONS

Dipartimento di Ingegneria Chimica Materiali Ambiente, Sapienza Università di Roma, Via Eudossiana 18, Roma, Italy

<sup>a)</sup>Electronic mail: [claudia.venditti@uniroma1.it](mailto:claudia.venditti@uniroma1.it)

<sup>b)</sup>Electronic mail: [massimiliano.giona@uniroma1.it](mailto:massimiliano.giona@uniroma1.it)

<sup>c)</sup>Author to whom correspondence should be addressed: [alessandra.adrover@uniroma1.it](mailto:alessandra.adrover@uniroma1.it)

## ABSTRACT

The paper develops a robust and computationally efficient homogenization approach, grounded on exact local and integral moments, to investigate the temporal evolution of effective dispersion properties of solute particles in periodic media possessing adsorbing/desorbing walls. Adsorption onto and desorption from active walls allow linear and reversible mass transfer between the solid surface and the fluid phase. The transient analysis reveals some important features of the dispersion process that cannot be captured by asymptotic approaches aimed at determining exclusively the long-range/large-distance dispersion properties. Two case studies are considered: the dispersion of an analyte in a sinusoidal channel with adsorbing/desorbing walls and the retentive pillar array column for liquid chromatography. For both systems, the transient analysis shows how the tortuous fluid motion induced by the sinusoidal walls or by the presence of pillars induces wide and persistent temporal oscillations of the effective velocity and dispersion coefficient even for a steady (non-pulsating) Stokes flow. The adsorption/desorption process strongly amplifies the phenomenon of the overshoot for the effective dispersion coefficient that, on short/intermediate time scales, reaches values significantly larger than the asymptotic one. Moreover, the method proposed allows a detailed analysis of the temporal evolution of the skewness of the marginal distribution of the analyte along the main stream direction. It clearly shows that the time scale for achieving the macro-transport regime, which implies a Gaussian (symmetric) marginal pdf, is largely underestimated if one bases the analysis on the attainment of constant asymptotic values for the effective velocity and for the dispersion coefficient.

Published under an exclusive license by AIP Publishing. <https://doi.org/10.1063/5.0130648>

## I. INTRODUCTION

The study of the transient behavior of dispersion properties is gaining more and more attention in connection with the development of microfluidic devices for separation<sup>1–6,20</sup> and mixing purposes.<sup>7–9</sup> The miniaturization of analytical devices, reducing the device dimension, solvent consumption and analysis time, has moved the attention toward the analysis and characterization of the transient behavior of dispersion properties because asymptotic conditions are not always achieved on the length-scales of the device.<sup>10–12</sup> Moreover, when the time scales of experimental observations reduce together with the device dimensions, the accurate description of transient phenomena becomes more and more important for a correct interpretation of experimental results.<sup>13,14</sup>

Multiple-scale expansion,<sup>15,38</sup> volume averaging,<sup>16–18</sup> and Brenner's moment analysis<sup>19</sup> are all equivalent strategies<sup>20–22</sup> for identifying the

long-term properties of advecting-diffusing fields, i.e., for reducing a transport problem, in its asymptotic regime, from the indefinite propagation in  $\mathbb{R}^n$  to a cell problem in a bounded domain  $\Omega \in \mathbb{R}^n$ .

In a series of recent papers,<sup>23–25</sup> we extended the potentialities of the Brenner's theory,<sup>19,26</sup> and proposed a theoretical approach based on exact moment analysis for generic  $n$ -dimensional periodic structures with solid impermeable obstacles, yielding exact results for the asymptotic values as well as for the transient dynamics of the effective transport parameters, for point-sized and finite-sized particles.

In this paper, we further extend the exact moment approach to include the presence of adsorbing-desorbing walls,<sup>27–30</sup> to investigate transient solute dispersion in chromatographic columns where reversible/irreversible adsorption is the driving force for the separation. The approach proposed is specifically suited for the transient analysis of a reversible reaction that allows both adsorption and desorption with

linear transfer rates,<sup>31,32</sup> but it also permits to investigate, as limiting cases, an infinitely fast adsorption/desorption process (local equilibrium condition) as well as a first order irreversible adsorption reaction.<sup>33–38</sup>

The method proposed allows to investigate the transient behavior of dispersion properties in any device in which periodic 2D or 3D unit cells can be identified, overcoming the limitation of dealing with straight channels (translationally invariant system) with a constant or slowly axially varying cross section.<sup>37,39–45</sup> The transient analysis is not limited to first and second order moments but includes also third-order moments.<sup>38,46,47</sup> Indeed, the evaluation of the degree of symmetry of a particle marginal distribution is essential for characterizing the transitional phase (preasymptotic regime<sup>48–50</sup>). The transient analysis permits a proper estimate of time/length to achieve the macrotransport/asymptotic regime<sup>34,37,51</sup> and how these time and length scales are influenced by the adsorption/desorption dynamics and by the inlet conditions.<sup>36</sup> The exact moment method can be applied to any steady or time-periodic velocity field,<sup>27,52</sup> be it solenoidal, irrotational, or a superposition of the two. Therefore, it allows to investigate transient and asymptotic dispersion properties in hydromagnetic/electrokinetic flows<sup>53,54</sup> as well as Casson fluid flows<sup>35,55</sup> usually adopted in hemodynamics.

The presence of adsorbing/desorbing walls requires the introduction and description of the space-time evolution of exact local moments in both the mobile and adsorbed phase. From exact local moments, it is possible to investigate the time-dependent dispersion features of the solute distribution in the two phases and how these are influenced by transport parameters, such as the solute diffusivity and the local adsorption/desorption transfer rates.

The exact moment approach is here applied to investigate the time-dependent behavior of dispersion properties of a single solute in a sinusoidal tube with reacting walls. Indeed, sinusoidal tubes represent one of the most investigated geometries, introduced to describe the influence of section narrowing/widening on transport phenomena in a variety of contexts as fractures, nanotubes,<sup>56</sup> zeolites,<sup>57</sup> cell biology,<sup>58</sup> blood vessels,<sup>59</sup> entropic barrier/entropic trap.<sup>3,60–75</sup> Moreover, sinusoidal tubes are also widely investigated as models for stenosed arteries in hemodynamics and the presence of reactive walls is relevant to describe oxygen transport and atherogenesis (see Refs. 35 and 55 and references therein). In this work, a Newtonian fluid is considered, but a non-Newtonian viscoelastic fluid (Casson) can be investigated as well within the framework of the proposed moment approach.

The paper also addresses the transient analysis of dispersion properties in a retentive pillar array column for liquid chromatography.<sup>18,30</sup> For both systems, the transient analysis shows how the tortuous fluid motion, induced by the sinusoidal walls or by the presence of pillars, causes wide and persistent temporal oscillations of the effective velocity and dispersion coefficient even for a steady (non-pulsating) Stokes flow. Moreover, the transient analysis shows that the phenomenon of the overshoot for the effective dispersion coefficient, already observed numerically and experimentally for non-reactive straight and sinusoidal tubes,<sup>60,76–79</sup> is largely amplified by the adsorption/desorption process.

The article is organized as follows. Section II introduces the exact local and integral moments in the presence of adsorbing/desorbing walls and discusses how the temporal evolution of the effective velocity, dispersion tensor and skewness of the marginal distribution can be evaluated on the basis of the time-dependent exact lower-order moments. Section III derives the asymptotic expression for the

dispersion properties in the general case and in the specific case of no-slip boundary conditions for the fluid velocity field at the solid walls. Sections IV and V focus on the analysis of the influence of adsorption/desorption dynamics on the transient and asymptotic behavior of dispersion properties of a single solute in a sinusoidal channel and in the microdevice with retentive pillars. For both systems, a detailed analysis of the temporal evolution of the skewness of the marginal distribution of the analyte along the main stream direction allows for a deeper understanding and an accurate identification of the time scales for achieving the long-term/large-distance macrotransport regime in the presence of reactive walls.

## II. STATEMENT OF THE PROBLEM

We model the convection/diffusion transport of a single solute in a two-dimensional fluid domain  $\Sigma_f \subseteq \mathbb{R}^2$  in the presence a solid non-porous phase  $\Sigma_s = (\cup_{i=1}^N \Sigma_s^i)$  made by  $N$  solid obstacles  $\{\Sigma_s^i\}_{i=1}^N$  of any shape, whose global surface  $\partial\Sigma_s$  is completely or partially coated with a thin adsorbing layer. Let  $\tilde{\Delta} \subseteq \partial\Sigma_s$  be the absorbing portion of  $\partial\Sigma_s$  and  $\Delta$  the non-adsorbing one, such that  $\tilde{\Delta} \cup \Delta = \partial\Sigma_s$  (see Fig. 1). Adsorption onto and desorption from  $\tilde{\Delta}$  allow linear and reversible mass transfer between the solid surface and the fluid phase. It is assumed that there is no drift and surface diffusion<sup>80,81</sup> of the analyte on  $\partial\Sigma_s$ .

Let  $\mathbf{v}(\mathbf{x})$  be the flow field of a solvent (compressible or incompressible) laden with the analyte and  $\mathbf{D}(\mathbf{x})$  the position-dependent diffusion tensor of the analyte. The transport equations for the normalized concentration  $p(\mathbf{x}, t)$  in the mobile (fluid) phase  $\Sigma_f = \mathbb{R}^2 - \Sigma_s$  and  $\tilde{p}(\tilde{\mathbf{x}}, t)$  in the stationary (adsorbed) phase  $\tilde{\Delta}$  read as follows:

$$\partial_t p(\mathbf{x}, t) = -\nabla \cdot (\mathbf{v}(\mathbf{x}) p) + \nabla \cdot (\mathbf{D}(\mathbf{x}) \nabla p), \quad (1)$$

$$(\mathbf{v}(\mathbf{x}) p - \mathbf{D}(\mathbf{x}) \nabla p) \cdot \mathbf{n}|_{\tilde{\Delta}} = (k_a(\tilde{\mathbf{x}}) p - k_d(\tilde{\mathbf{x}}) \tilde{p})|_{\tilde{\Delta}}, \quad (2)$$

$$(\mathbf{v}(\mathbf{x}) p - \mathbf{D}(\mathbf{x}) \nabla p) \cdot \mathbf{n}|_{\Delta} = 0, \quad (3)$$

$$\partial_t \tilde{p}(\tilde{\mathbf{x}}, t) = (k_a(\tilde{\mathbf{x}}) p - k_d(\tilde{\mathbf{x}}) \tilde{p})|_{\tilde{\Delta}}, \quad (4)$$

with the normalization condition

$$\int_{\Sigma_f} p(\mathbf{x}, t) d\mathbf{x} + \int_{\tilde{\Delta}} \tilde{p}(\tilde{\mathbf{x}}, t) d\tilde{\mathbf{x}} = 1. \quad (5)$$

In Eqs. (1)–(4),  $\mathbf{x}$  is any point in the mobile phase  $\Sigma_f$ ,  $\tilde{\mathbf{x}}$  any point on the adsorbing surface  $\tilde{\Delta}$ , and  $\tilde{\mathbf{x}}$  any point on the non-adsorbent part  $\Delta$  of the boundary, where impermeability conditions apply, Eq. (3).

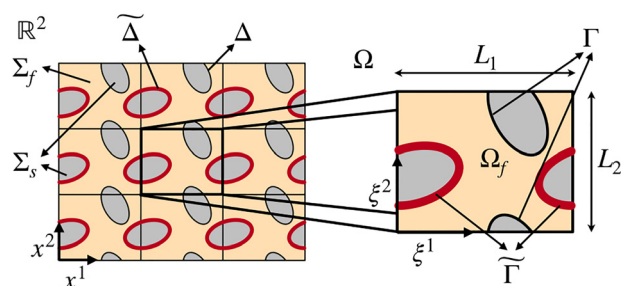


FIG. 1. Schematic representation of the infinite domain and of the orthogonal Cartesian unit cell. Red boundaries indicate the adsorbing/desorbing surfaces.

$k_a(\tilde{\mathbf{x}})$  [m/s] and  $k_d(\tilde{\mathbf{x}})$  [1/s] are the position-dependent adsorption and desorption kinetic constants, respectively.

Let us assume that  $\mathbf{v}(\mathbf{x})$  and  $\mathbf{D}(\mathbf{x})$ , as well as  $k_a(\tilde{\mathbf{x}})$  and  $k_d(\tilde{\mathbf{x}})$  are spatially periodic over a unit lattice cell  $\Omega$ ,

$$\begin{aligned} v^i(\mathbf{x} + m^1 L_1 \mathbf{e}_1 + m^2 L_2 \mathbf{e}_2) &= v^i(\mathbf{x}), \quad \forall m^1, m^2 \in \mathbb{Z}, \\ D^{ij}(\mathbf{x} + m^1 L_1 \mathbf{e}_1 + m^2 L_2 \mathbf{e}_2) &= D^{ij}(\mathbf{x}) \quad \text{for } i, j = 1, 2, \\ k_a(\tilde{\mathbf{x}} + m^1 L_1 \mathbf{e}_1 + m^2 L_2 \mathbf{e}_2) &= k_a(\tilde{\mathbf{x}}), \\ k_d(\tilde{\mathbf{x}} + m^1 L_1 \mathbf{e}_1 + m^2 L_2 \mathbf{e}_2) &= k_d(\tilde{\mathbf{x}}), \end{aligned} \tag{6}$$

where  $\mathbf{x} = (x^1, x^2)$  are orthogonal Cartesian coordinates and  $L_1$  and  $L_2$  are the periodicity lengths along the unit lattice vector  $\mathbf{e}_1, \mathbf{e}_2$ .

The scope of dispersion theory is to derive the asymptotic effective transport parameters, namely the entries of the effective velocity field  $\mathcal{V}_\infty^i$  and the entries of the effective symmetric dispersion tensor  $\mathcal{D}_\infty^{ij}$ , entering the constant-coefficient advection-diffusion equation,

$$\partial_t \bar{p} = -\mathcal{V}_\infty^i \partial_{X_i} \bar{p} + \mathcal{D}_\infty^{ij} \partial_{X_i} \partial_{X_j} \bar{p}, \tag{7}$$

describing the long-time/large-distance limit of the transport Eqs. (1)–(4), defined on  $\mathbb{R}^2$  and possessing periodic coefficients on the unit cell  $\Omega$ . In Eq. (7), the  $X^i, i = 1, 2$  are the long-range spatial variables and  $\bar{p}(\mathbf{X}, t)$  is the long-range field representing the mean value of the solute concentration (in both the mobile and adsorbed phase) averaged over the periodicity cell  $\Omega$ . We limit our analysis to two-dimensional systems because  $\mathbb{R}^2$  is the minimal space in which the tensorial nature of the dispersion tensor can be appreciated. The extension to higher dimensions is straightforward. In Eq. (7) and throughout the paper, Einstein's sum convention over repeated indexes has been adopted.

Moment analysis allows to derive the effective transport parameters from the properties of the periodic fields  $v^i(\mathbf{x})$  and  $D^{ij}(\mathbf{x})$ , thus transferring the analysis of the transport problem from  $\mathbb{R}^2$  into a cell problem defined in the periodicity cell  $\Omega$ . This task can be accomplished by decoupling the spatial variables into local and global coordinates and using the spatial moments of  $p(\mathbf{x}, t)$  and  $\tilde{p}(\tilde{\mathbf{x}}, t)$ .

Indeed, the asymptotic effective transport parameters  $\mathcal{V}_\infty^i$  and  $\mathcal{D}_\infty^{ij}$  can be estimated from the asymptotic behavior of the lower-order terms of the integral moment hierarchy  $\{M_{q_1, q_2}^{(q)}(t)\}$  defined as follows:

$$\begin{aligned} M_{q_1, q_2}^{(q)}(t) &= \int_{\Sigma_f} (x^1)^{q_1} (x^2)^{q_2} p(\mathbf{x}, t) d\mathbf{x} + \int_{\tilde{\Delta}} (\tilde{x}^1)^{q_1} (\tilde{x}^2)^{q_2} \tilde{p}(\tilde{\mathbf{x}}, t) d\tilde{\mathbf{x}}, \\ q_1, q_2 &= 0, 1, \dots, \infty, \quad q = q_1 + q_2, \end{aligned} \tag{8}$$

where  $M_{q_1, q_2}^{(q)}(t)$  is the  $q$ -th order integral moment of the normalized solute concentration in both fluid and adsorbed phase.

Starting from Eq. (8), the time-dependent effective transport parameters can be defined and evaluated as follows:

$$\mathcal{V}_\infty^1(t) = d_t M_{1,0}^{(1)}, \quad \mathcal{V}_\infty^2(t) = d_t M_{0,1}^{(1)}, \tag{9}$$

$$\mathcal{D}_\infty^{1,1}(t) = \frac{1}{2} d_t (\sigma_{2,0}^2) = \frac{1}{2} d_t (M_{2,0}^{(2)} - (M_{1,0}^{(1)})^2) = \frac{d_t M_{2,0}^{(2)}}{2} - M_{1,0}^{(1)} \mathcal{V}_\infty^1(t), \tag{10}$$

$$\mathcal{D}_\infty^{2,2}(t) = \frac{1}{2} d_t (\sigma_{0,2}^2) = \frac{1}{2} d_t (M_{0,2}^{(2)} - (M_{0,1}^{(1)})^2) = \frac{d_t M_{0,2}^{(2)}}{2} - M_{0,1}^{(1)} \mathcal{V}_\infty^2(t), \tag{11}$$

$$\mathcal{D}_\infty^{1,2}(t) = \mathcal{D}_\infty^{2,1}(t) = \frac{1}{2} d_t (\sigma_{1,1}^2) = \frac{1}{2} (d_t M_{1,1}^{(2)} - M_{1,0}^{(1)} \mathcal{V}_\infty^2(t) - M_{0,1}^{(1)} \mathcal{V}_\infty^1(t)). \tag{12}$$

The time-dependent effective velocity  $\mathcal{V}^i(t)$ , Eq. (9), represents the  $i$ -th component of the instantaneous velocity of the center of mass of the total solute distribution.  $\mathcal{V}^i(t)$  asymptotically converges toward the effective velocity component  $\mathcal{V}_\infty^i$ , entering the long-time/large-distance macrotransport model Eq. (7). Correspondingly, the time-dependent coefficients  $\mathcal{D}^{1,1}(t)$  and  $\mathcal{D}^{2,2}(t)$  are an indirect measure of the instantaneous variances  $\sigma_{2,0}^2$  and  $\sigma_{0,2}^2$  of the marginal probability density functions  $F_1(x^1, t)$  and  $F_2(x^2, t)$ , where  $F_i(x^i, t) dx^i$  represents the fraction of solute particles (in both the mobile and adsorbed phase) falling in the range  $(x^i, x^i + dx^i)$ , regardless of the solute particle position in the  $x^j, j \neq i$  direction. Each component  $\mathcal{D}^{ij}(t)$  asymptotically converges toward  $\mathcal{D}_\infty^{ij}$ , entering Eq. (7).

Third-order moments  $M_{3,0}^{(3)}(t)$  and  $M_{0,3}^{(3)}(t)$  allow the estimate of the time-dependent skewness  $sk^{(1,1)}(t)$  and  $sk^{(2,2)}(t)$  of the marginal pdfs  $F_1(x^1, t)$  and  $F_2(x^2, t)$ , respectively,

$$sk^{(1,1)}(t) = \frac{\mu_{3,0}}{(\sigma_{2,0}^2)^{3/2}} = \frac{M_{3,0}^{(3)} + 3M_{2,0}^{(2)}M_{1,0}^{(1)} - 2(M_{1,0}^{(1)})^3}{(M_{2,0}^{(2)} - (M_{1,0}^{(1)})^2)^{3/2}}, \tag{13}$$

$$sk^{(2,2)}(t) = \frac{\mu_{0,3}}{(\sigma_{0,2}^2)^{3/2}} = \frac{M_{0,3}^{(3)} + 3M_{0,2}^{(2)}M_{0,1}^{(1)} - 2(M_{0,1}^{(1)})^3}{(M_{0,2}^{(2)} - (M_{0,1}^{(1)})^2)^{3/2}}. \tag{14}$$

Here,  $\mu_{3,0}$  and  $\mu_{0,3}$  are the corresponding third-order centered moments. Both  $sk^{(1,1)}(t)$  and  $sk^{(2,2)}(t)$  converge toward zero and the time  $t^*$  at which  $|sk^{(1,1)}(t^*)|$  and  $|sk^{(2,2)}(t^*)|$  become sufficiently small, order  $\mathcal{O}(0.1)$ , can be assumed as the characteristic time of achievement of asymptotic conditions when the macrotransport Eq. (7) holds true.

The possibility of evaluating all the time-dependent quantities  $\mathcal{V}^i(t)$ ,  $\mathcal{D}^{ij}(t)$ , and  $sk^{(i,i)}(t)$  is intrinsically related to the possibility of having an “exact” representation of the integral moment hierarchy  $\{M_{q_1, q_2}^{(q)}(t)\}$  Eq. (8) in terms of local variables defined onto the unit cell  $\Omega$ .

Let  $(\xi^1, \xi^2)$  be the local coordinates of the unit lattice cell  $\Omega$ ,  $0 \leq \xi^1 \leq L_1$ ,  $0 \leq \xi^2 \leq L_2$ . Any point  $\mathbf{x} \in \mathbb{R}^2$ , including boundary points belonging to  $\partial\Sigma_s$ , can be uniquely specified as follows:

$$\mathbf{x} = (\xi^1 + m^1 L_1) \mathbf{e}_1 + (\xi^2 + m^2 L_2) \mathbf{e}_2 = \boldsymbol{\xi} + \mathbf{x}_m, \tag{15}$$

where the following compact notation  $\boldsymbol{\xi} = (\xi^1, \xi^2)$ ,  $\mathbf{x}_m = m^1 L_1 \mathbf{e}_1 + m^2 L_2 \mathbf{e}_2$ ,  $\mathbf{m} = (m^1, m^2)$ , has been adopted. See Fig. 1 for a schematic representation of the unit cell and the system of local coordinates defined on it.

Substituting the expression Eq. (15) for the global coordinates  $\mathbf{x}$  into Eq. (8), the exact integral moments  $M_{q_1, q_2}^{(q)}(t)$  can be written as follows:

$$\begin{aligned} M_{q_1, q_2}^{(q)}(t) &= \sum_{\mathbf{m}} \int_{\Omega_f} (\xi^1 + m^1 L_1)^{q_1} (\xi^2 + m^2 L_2)^{q_2} p(\boldsymbol{\xi} + \mathbf{x}_m, t) d\boldsymbol{\xi} \\ &\quad + \sum_{\mathbf{m}} \int_{\tilde{\Gamma}} (\tilde{\xi}^1 + m^1 L_1)^{q_1} (\tilde{\xi}^2 + m^2 L_2)^{q_2} \tilde{p}(\tilde{\boldsymbol{\xi}} + \mathbf{x}_m, t) d\tilde{\boldsymbol{\xi}} \\ &= \int_{\Omega_f} P_{q_1, q_2}^{(q)}(\boldsymbol{\xi}, t) d\boldsymbol{\xi} + \int_{\tilde{\Gamma}} \tilde{P}_{q_1, q_2}^{(q)}(\tilde{\boldsymbol{\xi}}, t) d\tilde{\boldsymbol{\xi}}, \end{aligned} \tag{16}$$

where  $\Omega_f$  is the portion of the unit cell occupied by the fluid phase,  $\Gamma$  and  $\tilde{\Gamma}$  the non-adsorbing and the adsorbing portions of the solid

boundary, respectively. The exact *local* moments  $P_{q_1,q_2}^{(q)}(\xi, t)$  in the mobile phase and  $\tilde{P}_{q_1,q_2}^{(q)}(\tilde{\xi}, t)$  in the adsorbed phase, defined on the unit cell  $\Omega$  and entering Eq. (16) for the global integral moments  $M_{q_1,q_2}^{(q)}(t)$ , are the key quantities to be estimated for the evaluation of the effective time-dependent transport parameters  $\mathcal{V}^i(t)$ ,  $\mathcal{D}^{ij}(t)$ , and  $sk^{(i,i)}(t)$ .

If one is interested exclusively in the asymptotic values  $\mathcal{V}_\infty^i$  and  $\mathcal{D}_\infty^{ij}$ , then quantized local moments  $Q_{q_1,q_2}^{(q)}(\xi, t)$ ,  $\tilde{Q}_{q_1,q_2}^{(q)}(\tilde{\xi}, t)$  and integral moments  $N_{q_1,q_2}^{(q)}(t)$  can be defined according to Brenner's approach,

$$\begin{aligned} Q_{q_1,q_2}^{(q)}(\xi, t) &= (m^1 L_1)^{q_1} (m^2 L_2)^{q_2} p(\xi + \mathbf{x}_m, t), \\ \tilde{Q}_{q_1,q_2}^{(q)}(\tilde{\xi}, t) &= (m^1 L_1)^{q_1} (m^2 L_2)^{q_2} \tilde{p}(\tilde{\xi} + \mathbf{x}_m, t), \\ N_{q_1,q_2}^{(q)}(t) &= \int_{\Omega_f} Q_{q_1,q_2}^{(q)}(\xi, t) d\xi + \int_{\tilde{\Gamma}} \tilde{Q}_{q_1,q_2}^{(q)}(\tilde{\xi}, t) d\tilde{\xi}. \end{aligned} \tag{17}$$

The definition Eq. (17) of integral moments fits into an asymptotic theory of transport. It is, however, not fully rigorous and allows only for the estimate of asymptotic effective transport parameters. Indeed, it is rather straightforward to verify that  $N_{q_1,q_2}^{(q)}(t) \neq M_{q_1,q_2}^{(q)}(t)$  and that only the exact local moments  $P_{q_1,q_2}^{(q)}(\xi, t)$  and  $\tilde{P}_{q_1,q_2}^{(q)}(\tilde{\xi}, t)$  defined in Eq. (16) are such that their integral over the periodicity cell  $\Omega$  coincide, at any time  $t > 0$ , with the expressions of the corresponding moments of  $p(\mathbf{x}, t)$  and  $\tilde{p}(\tilde{\mathbf{x}}, t)$  defined by Eq. (8).

Section II A is devoted to the analysis of the space-time evolution of exact local moments and to the evaluation of time-dependent effective transport parameters  $\mathcal{V}^i(t)$ ,  $\mathcal{D}^{ij}(t)$  and  $sk^{(i,i)}(t)$ .

### A. Space-time evolution of exact local and integral moments

From the original transport model Eqs. (1)–(4), by enforcing the definition Eq. (16) for the local moments  $P_{q_1,q_2}^{(q)}(\xi, t)$  and  $\tilde{P}_{q_1,q_2}^{(q)}(\tilde{\xi}, t)$  for any  $q_1 \geq 0$ ,  $q_2 \geq 0$ ,  $q = (q_1 + q_2) \geq 0$ , one obtains the following transport equation for the hierarchy of local moments:

$$\begin{aligned} \partial_t P_{q_1,q_2}^{(q)}(\xi, t) &= \mathcal{L}_\xi [P_{q_1,q_2}^{(q)}] + q_1 \left[ v^1 P_{q_1-1,q_2}^{(q-1)} \right. \\ &\quad \left. - \partial_{\xi_j} (D^{1,j} P_{q_1-1,q_2}^{(q-1)}) - D^{1,j} \partial_{\xi_j} (P_{q_1-1,q_2}^{(q-1)}) \right] \\ &\quad + q_2 \left[ v^2 P_{q_1,q_2-1}^{(q-1)} - \partial_{\xi_j} (D^{2,j} P_{q_1,q_2-1}^{(q-1)}) \right. \\ &\quad \left. - D^{2,j} \partial_{\xi_j} (P_{q_1,q_2-1}^{(q-1)}) \right] + 2q_1 q_2 D^{1,2} P_{q_1-1,q_2-1}^{(q-2)} \\ &\quad + q_1 (q_1 - 1) D^{1,1} P_{q_1-2,q_2}^{(q-2)} \\ &\quad + q_2 (q_2 - 1) D^{2,2} P_{q_1,q_2-2}^{(q-2)} \quad \forall \xi \in \Omega_f, \end{aligned} \tag{18}$$

$$\partial_t \tilde{P}_{q_1,q_2}^{(q)}(\tilde{\xi}, t) = k_a P_{q_1,q_2}^{(q)}(\tilde{\xi}, t) - k_d \tilde{P}_{q_1,q_2}^{(q)}(\tilde{\xi}, t) \quad \forall \tilde{\xi} \in \tilde{\Gamma}, \tag{19}$$

where  $\mathcal{L}_\xi[\cdot]$  is the cell advection-diffusion operator,

$$\mathcal{L}_\xi[g(\xi)] = -\partial_{\xi_i} (v^i(\xi) g(\xi)) + \partial_{\xi_i} (D^{i,j}(\xi) \partial_{\xi_j} g(\xi)) = -\nabla \cdot \mathbf{J}[g(\xi)], \tag{20}$$

and  $\mathbf{J}[\cdot]$  is the flux operator,

$$\mathbf{J}^i[g(\xi)] = v^i g(\xi) - D^{i,j} \partial_{\xi_j} g(\xi) \quad i = 1, 2. \tag{21}$$

The local moments in the mobile phase  $P_{q_1,q_2}^{(q)}$  satisfy periodic conditions on the boundaries of the periodic cell not occupied by solid obstacles, i.e., on  $\partial\Omega \cap \partial\Omega_f$ , and the following boundary conditions on  $\Gamma$  and  $\tilde{\Gamma}$ :

$$\mathbf{J} \left[ P_{q_1,q_2}^{(q)} \right] \cdot \mathbf{n}|_{\tilde{\xi}} = -(q_1 D^{1,i} P_{q_1-1,q_2}^{(q-1)} + q_2 D^{2,i} P_{q_1,q_2-1}^{(q-1)}) (\mathbf{e}_i \cdot \mathbf{n})|_{\tilde{\xi}}, \quad \forall \tilde{\xi} \in \Gamma, \tag{22}$$

$$\mathbf{J} \left[ P_{q_1,q_2}^{(q)} \right] \cdot \mathbf{n}|_{\tilde{\xi}} = -(q_1 D^{1,i} P_{q_1-1,q_2}^{(q-1)} + q_2 D^{2,i} P_{q_1,q_2-1}^{(q-1)}) (\mathbf{e}_i \cdot \mathbf{n})|_{\tilde{\xi}} + k_a P_{q_1,q_2}^{(q)}(\tilde{\xi}, t) - k_d \tilde{P}_{q_1,q_2}^{(q)}(\tilde{\xi}, t), \quad \forall \tilde{\xi} \in \tilde{\Gamma}, \tag{23}$$

the latter boundary condition (23) linking together the two sets of local moments in the two phases.

By further integrating Eq. (18) for  $P_{q_1,q_2}^{(q)}$  over the fluid domain  $\Omega_f$  and Eq. (19) for  $\tilde{P}_{q_1,q_2}^{(q)}$  over the adsorbed phase domain  $\tilde{\Gamma}$ , and enforcing the boundary conditions for  $P_{q_1,q_2}^{(q)}$ , one arrives to the following equation for the total time-dependent integral moments  $M_{q_1,q_2}^{(q)}(t)$ ,

$$\begin{aligned} d_t M_{q_1,q_2}^{(q)} &= q_1 \underbrace{\left[ \int_{\Omega_f} v^1 P_{q_1-1,q_2}^{(q-1)} - D^{1,j} \partial_{\xi_j} (P_{q_1-1,q_2}^{(q-1)}) d\xi \right]}_{q_1 J^1 [P_{q_1-1,q_2}^{(q-1)}]} \\ &\quad + q_2 \underbrace{\left[ \int_{\Omega_f} v^2 P_{q_1,q_2-1}^{(q-1)} - D^{2,j} \partial_{\xi_j} (P_{q_1,q_2-1}^{(q-1)}) d\xi \right]}_{q_2 J^2 [P_{q_1,q_2-1}^{(q-1)}]} \\ &\quad + 2 q_1 q_2 \int_{\Omega_f} D^{1,2} P_{q_1-1,q_2-1}^{(q-2)} d\xi \\ &\quad + q_1 (q_1 - 1) \int_{\Omega_f} D^{1,1} P_{q_1-2,q_2}^{(q-2)} d\xi \\ &\quad + q_2 (q_2 - 1) \int_{\Omega_f} D^{2,2} P_{q_1,q_2-2}^{(q-2)} d\xi. \end{aligned} \tag{24}$$

It is worth noting that exactly the same Eq. (24) is obtained if the adsorbing layer is absent. However, the adsorption/desorption kinetics is implicitly influencing the temporal evolution of the integral moments because the local moments  $P_{q_1,q_2}^{(q)}$  in the mobile phase interact with the local moments  $\tilde{P}_{q_1,q_2}^{(q)}$  in the adsorbed phase through the boundary condition Eq. (23).

The same observation applies for the temporal evolution of the effective velocities that, according to their definition Eq. (9), read as follows:

$$\mathcal{V}^i(t) = \int_{\Omega_f} J^i [P_{0,0}^{(0)}] d\xi = \int_{\Omega_f} (v^i P_{0,0}^{(0)} - D^{i,j} \partial_{\xi_j} (P_{0,0}^{(0)})) d\xi \quad i = 1, 2, \tag{25}$$

thus involving exclusively the zeroth-order local moment  $P_{0,0}^{(0)}$  in the mobile phase, the latter satisfying an advection-diffusion equation

with no-flux boundary conditions on  $\Gamma$  and adsorptive boundary conditions on  $\tilde{\Gamma}$ ,

$$\partial_t P_{0,0}^{(0)} = \mathcal{L}_\xi [P_{0,0}^{(0)}], \tag{26}$$

$$\mathbf{J} [P_{0,0}^{(0)}] \cdot \mathbf{n}|_{\tilde{\xi}} = k_a P_{0,0}^{(0)}(\tilde{\xi}, t) - k_d \tilde{P}_{0,0}^{(0)}(\tilde{\xi}, t) \quad \forall \tilde{\xi} \in \tilde{\Gamma}, \tag{27}$$

$$\mathbf{J} [P_{0,0}^{(0)}] \cdot \mathbf{n}|_{\xi} = 0 \quad \forall \xi \in \Gamma. \tag{28}$$

On the contrary, the temporal evolution of the dispersion tensor entries  $\mathcal{D}^{ij}(t)$

$$\begin{aligned} \mathcal{D}^{1,1}(t) = & \int_{\Omega_f} [(v^1 - \mathcal{V}^1)P_{1,0}^{(1)} - D^{1,j}\partial_{\xi_j}(P_{1,0}^{(1)}) + D^{1,1}P_{0,0}^{(0)}] d\xi \\ & - \int_{\tilde{\Gamma}} \mathcal{V}^1 \tilde{P}_{1,0}^{(1)} d\tilde{\xi}, \end{aligned} \tag{29}$$

$$\begin{aligned} \mathcal{D}^{2,2}(t) = & \int_{\Omega_f} [(v^2 - \mathcal{V}^2)P_{0,1}^{(1)} - D^{2,j}\partial_{\xi_j}(P_{0,1}^{(1)}) + D^{2,2}P_{0,0}^{(0)}] d\xi \\ & - \int_{\tilde{\Gamma}} \mathcal{V}^2 \tilde{P}_{0,1}^{(1)} d\tilde{\xi}, \end{aligned} \tag{30}$$

$$\begin{aligned} \mathcal{D}^{1,2}(t) = & \int_{\Omega_f} \frac{1}{2} [(v^1 - \mathcal{V}^1)P_{0,1}^{(1)} + (v^2 - \mathcal{V}^2)P_{1,0}^{(1)} \\ & - D^{1,j}\partial_{\xi_j}(P_{0,1}^{(1)}) - D^{2,j}\partial_{\xi_j}(P_{1,0}^{(1)}) + 2D^{1,2}P_{0,0}^{(0)}] d\xi \\ & - \int_{\tilde{\Gamma}} \frac{1}{2} [\mathcal{V}^1 \tilde{P}_{0,1}^{(1)} + \mathcal{V}^2 \tilde{P}_{1,0}^{(1)}] d\tilde{\xi}, \end{aligned} \tag{31}$$

involves explicitly the zeroth- and first-order local moment  $P_{0,0}^{(0)}$ ,  $P_{1,0}^{(1)}$  and  $P_{0,1}^{(1)}$  in the mobile phase and the first-order local moments  $\tilde{P}_{1,0}^{(1)}$  and  $\tilde{P}_{0,1}^{(1)}$  in the adsorbed phase.

First- and second-order local moments in both the mobile and adsorbed phase are involved in the computation of the time-dependent skewness  $sk^{(1,1)}(t)$  and  $sk^{(2,2)}(t)$ , as they appear in the centered third-order moments,

$$\begin{aligned} d_t \mu_{3,0}^{(3)} = & 3 \int_{\Omega_f} [(v^1 - \mathcal{V}^1)P_{2,0}^{(2)} - D^{1,j}\partial_{\xi_j}P_{2,0}^{(2)}] d\xi \\ & + 6 \int_{\Omega_f} (D^{1,1} - \mathcal{D}^{1,1})P_{1,0}^{(1)} d\xi \\ & - \int_{\tilde{\Gamma}} [3\mathcal{V}^1 \tilde{P}_{2,0}^{(2)} + 6\mathcal{D}^{1,1} \tilde{P}_{1,0}^{(1)}] d\tilde{\xi}, \end{aligned} \tag{32}$$

$$\begin{aligned} d_t \mu_{0,3}^{(3)} = & 3 \int_{\Omega_f} [(v^2 - \mathcal{V}^2)P_{0,2}^{(2)} - D^{2,j}\partial_{\xi_j}P_{0,2}^{(2)}] d\xi \\ & + 6 \int_{\Omega_f} (D^{2,2} - \mathcal{D}^{2,2})P_{0,1}^{(1)} d\xi \\ & - \int_{\tilde{\Gamma}} [3\mathcal{V}^2 \tilde{P}_{0,2}^{(2)} + 6\mathcal{D}^{2,2} \tilde{P}_{0,1}^{(1)}] d\tilde{\xi}. \end{aligned} \tag{33}$$

A detailed analysis of the asymptotic properties, i.e., long-time/large distance features of local  $P_{q_1,q_2}^{(q)}$ ,  $\tilde{P}_{q_1,q_2}^{(q)}$  and integral  $M_{q_1,q_2}^{(q)}(t)$  moments, is presented in Sec. III. Section II B focuses on the analysis of dispersion

features in the fluid and adsorbed phase separately and analyze how they contribute to dispersion properties of the global solute distribution.

### B. Correlation between moments

The problem formulation outlined above, introducing and describing the space-time evolution of local moments of the fluid and adsorbed phases, allows to investigate the time-dependent dispersion features of the solute distribution in the two phases. Indeed, each integral moment  $M_{q_1,q_2}^{(q)}$  can be viewed as the summation of the two contributions,

$$\begin{aligned} M_{q_1,q_2}^{(q)}(t) = & m_{q_1,q_2}^{(q)}(t) m_{0,0}^{(0)}(t) + \tilde{m}_{q_1,q_2}^{(q)}(t) \tilde{m}_{0,0}^{(0)}(t), \\ m_{q_1,q_2}^{(q)}(t) = & \frac{\int_{\Omega_f} P_{q_1,q_2}^{(q)} d\xi}{\int_{\Omega_f} P_{0,0}^{(0)} d\xi}, \quad \tilde{m}_{q_1,q_2}^{(q)}(t) = \frac{\int_{\tilde{\Gamma}} \tilde{P}_{q_1,q_2}^{(q)} d\tilde{\xi}}{\int_{\tilde{\Gamma}} \tilde{P}_{0,0}^{(0)} d\tilde{\xi}}, \end{aligned} \tag{34}$$

where  $m_{q_1,q_2}^{(q)}$  and  $\tilde{m}_{q_1,q_2}^{(q)}$  are the integral moment of the particle density functions in the mobile and adsorbed phase, respectively, and the integral moment  $M_{q_1,q_2}^{(q)}$  is the convex combination of the single-phase integral moments  $m_{q_1,q_2}^{(q)}$  and  $\tilde{m}_{q_1,q_2}^{(q)}$  with weights  $m_{0,0}^{(0)}$  and  $\tilde{m}_{0,0}^{(0)}$  representing the fraction of solute particles in the mobile and adsorbed phase.

Starting from the single-phase integral moments, it is possible to define and compute the single-phase effective velocities,

$$\begin{aligned} v^1(t) = & d_t m_{1,0}^{(1)}, \quad \tilde{v}^1(t) = d_t \tilde{m}_{1,0}^{(1)}, \\ v^2(t) = & d_t m_{0,1}^{(1)}, \quad \tilde{v}^2(t) = d_t \tilde{m}_{0,1}^{(1)}, \end{aligned} \tag{35}$$

where  $v^i(t)$  are the velocity components of the center of mass of solute particles in the mobile phase while  $\tilde{v}^i(t)$  refer to the solute particles in the adsorbed phase.

Similarly, the variances  $\beta_{i,i}^2$  and  $\tilde{\beta}_{i,i}^2$  and the effective dispersion tensors  $\mathcal{d}^{i,i}$  and  $\tilde{\mathcal{d}}^{i,i}$  associated with the particle density function in the mobile and adsorbed phase can be defined as follows:

$$\begin{aligned} \mathcal{d}^{1,1}(t) = & \frac{1}{2} \mathcal{d}_t (\beta_{2,0}^2) = \frac{1}{2} \mathcal{d}_t (m_{2,0}^{(2)} - (m_{1,0}^{(1)})^2), \\ \tilde{\mathcal{d}}^{1,1}(t) = & \frac{1}{2} \mathcal{d}_t (\tilde{\beta}_{2,0}^2) = \frac{1}{2} \mathcal{d}_t (\tilde{m}_{2,0}^{(2)} - (\tilde{m}_{1,0}^{(1)})^2), \end{aligned} \tag{36}$$

$$\begin{aligned} \mathcal{d}^{2,2}(t) = & \frac{1}{2} \mathcal{d}_t (\beta_{0,2}^2) = \frac{1}{2} \mathcal{d}_t (m_{0,2}^{(2)} - (m_{0,1}^{(1)})^2), \\ \tilde{\mathcal{d}}^{2,2}(t) = & \frac{1}{2} \mathcal{d}_t (\tilde{\beta}_{0,2}^2) = \frac{1}{2} \mathcal{d}_t (\tilde{m}_{0,2}^{(2)} - (\tilde{m}_{0,1}^{(1)})^2). \end{aligned} \tag{37}$$

From Eq. (35), it is possible to derive an explicit relationship between the effective velocity  $\mathcal{V}^i$  of the global solute distribution and the single-phase effective velocities  $v^i$  and  $\tilde{v}^i$ . For example, for  $\mathcal{V}^1$  one obtains

$$\mathcal{V}^1 = [v^1 m_{0,0}^{(0)} + \tilde{v}^1 \tilde{m}_{0,0}^{(0)}] + [m_{1,0}^{(1)} \mathcal{d}_t m_{0,0}^{(0)} + \tilde{m}_{1,0}^{(1)} \mathcal{d}_t \tilde{m}_{0,0}^{(0)}], \tag{38}$$

where the first term between brackets is the convex combination of the single-phase velocities and the second term quantifies how the interaction between the two phases contributes to the effective velocity of the global particle density function. By enforcing the conservation

constrain  $m_{0,0}^{(0)} + \tilde{m}_{0,0}^{(0)} = 1$ , the interaction term can be rewritten as follows:

$$h_1(t) = [m_{1,0}^{(1)} d_t m_{0,0}^{(0)} + \tilde{m}_{1,0}^{(1)} d_t \tilde{m}_{0,0}^{(0)}] = [m_{1,0}^{(1)} - \tilde{m}_{1,0}^{(1)}] d_t m_{0,0}^{(0)}. \quad (39)$$

For any initial condition in which the solute is entirely in the fluid phase, the solute fraction in the fluid phase is always a decreasing function of time, i.e.,  $d_t m_{0,0}^{(0)} < 0 \forall t$ . It asymptotically converges to the constant value  $\lim_{t \rightarrow \infty} m_{0,0}^{(0)} = c_0$ ,  $c_0$  representing the fraction of solute particles in the mobile phase when dynamic equilibrium conditions are reached. Simultaneously,  $\lim_{t \rightarrow \infty} \tilde{m}_{0,0}^{(0)} = \tilde{c}_0$ ,  $\tilde{c}_0$  representing the asymptotic fraction of solute particles in the adsorbed phase,  $c_0 + \tilde{c}_0 = 1$ . Therefore, by considering that  $d_t m_{0,0}^{(0)} \rightarrow 0$  and  $|m_{1,0}^{(1)}| > |\tilde{m}_{1,0}^{(1)}|$ , the interaction term has always an opposite sign with respect to  $\mathcal{V}^1$ . The interaction between the fluid and adsorbed phases results in an effective velocity of the global solute distribution that is smaller, in absolute value, than the convex combination of the single-phase velocities. Moreover, since the interaction term asymptotically converges to 0, on the long term-large distance limit when dynamic equilibrium conditions are reached, all the velocities coincide, i.e.,  $\mathcal{V}_\infty^1 = v_\infty^1 = \tilde{v}_\infty^1$  as the swarm of solute particle in the mobile and adsorbed phase are traveling at the same speed.

A similar analysis can be performed for the variance  $\sigma_{2,0}^2$  of the global solute distribution, that can be expressed as the convex combination of the single-phase variances ( $\beta_{2,0}^2$ ) and ( $\tilde{\beta}_{2,0}^2$ ) plus an always positive interaction term  $h_2(t)$ ,

$$\sigma_{2,0}^2 = [\beta_{2,0}^2 m_{0,0}^{(0)} + \tilde{\beta}_{2,0}^2 \tilde{m}_{0,0}^{(0)}] + \underbrace{[m_{0,0}^{(0)} \tilde{m}_{0,0}^{(0)} (\tilde{m}_{1,0}^{(1)} - m_{1,0}^{(1)})^2]}_{=h_2(t)}, \quad (40)$$

that asymptotically converges toward a positive constant value

$$\lim_{t \rightarrow \infty} h_2(t) = \lim_{t \rightarrow \infty} [m_{0,0}^{(0)} \tilde{m}_{0,0}^{(0)} (\tilde{m}_{1,0}^{(1)} - m_{1,0}^{(1)})^2] = c_0 \tilde{c}_0 (\tilde{c}_1 - c_1)^2, \quad (41)$$

because  $\lim_{t \rightarrow \infty} m_{1,0}^{(1)} = v_\infty^1 t + c_1$ ,  $\lim_{t \rightarrow \infty} \tilde{m}_{1,0}^{(1)} = \tilde{v}_\infty^1 t + \tilde{c}_1$  and  $v_\infty^1 = \tilde{v}_\infty^1$ . Therefore, the variance of the global particle density function is always larger than the convex combination of the single-phase variances. Equation (42) implies for the effective dispersion coefficient  $\mathcal{D}^{1,1}$ ,

$$\mathcal{D}^{1,1} = [d^{1,1} m_{0,0}^{(0)} + \tilde{d}^{1,1} \tilde{m}_{0,0}^{(0)}] + [\beta_{2,0}^2 d_t m_{0,0}^{(0)} + \tilde{\beta}_{2,0}^2 d_t \tilde{m}_{0,0}^{(0)} + d_t h_2]. \quad (42)$$

Since the interaction term  $h_2(t)$  is asymptotically constant, as well as  $m_{0,0}^{(0)}$  and  $\tilde{m}_{0,0}^{(0)}$ , it readily follows that when dynamic equilibrium conditions are reached, all the effective dispersion coefficients coincide, i.e.,

$$\mathcal{D}_\infty^{1,1} = [d_\infty^{1,1} c_0 + \tilde{d}_\infty^{1,1} \tilde{c}_0] \Rightarrow \mathcal{D}_\infty^{1,1} = d_\infty^{1,1} = \tilde{d}_\infty^{1,1}. \quad (43)$$

The same analysis can be performed for  $\mathcal{V}^2$  and  $\mathcal{D}^{2,2}$ .

### III. ASYMPTOTIC ANALYSIS

In the long-time/large-distance limit, we assume that dynamic equilibrium conditions are reached, so that the fraction of solute particles in the mobile phase (and therefore also in the adsorbed phase) of the unit cell  $\Omega$  no longer changes over time, this implying

$$\lim_{t \rightarrow \infty} \int_{\Omega_f} \partial_t P_{0,0}^{(0)}(\xi, t) d\xi \rightarrow 0, \quad \lim_{t \rightarrow \infty} \int_{\tilde{\Gamma}} \partial_t \tilde{P}_{0,0}^{(0)}(\tilde{\xi}, t) d\tilde{\xi} \rightarrow 0. \quad (44)$$

As a direct consequence of Eq. (44), in the long term,  $P_{0,0}^{(0)}$  and  $\tilde{P}_{0,0}^{(0)}$  converge toward stationary functions  $w_0(\xi)$  and  $\tilde{w}_0(\tilde{\xi})$  satisfying the following pointwise relationship at the reactive boundary  $\tilde{\Gamma}$ ,

$$\lim_{t \rightarrow \infty} P_{0,0}^{(0)}(\xi, t) = w_0(\xi) \quad \lim_{t \rightarrow \infty} \tilde{P}_{0,0}^{(0)}(\tilde{\xi}, t) = \tilde{w}_0(\tilde{\xi}) = \frac{k_a(\tilde{\xi})}{k_d(\tilde{\xi})} w_0(\tilde{\xi}), \quad (45)$$

$w_0(\xi)$  being the Frobenius eigenfunction of the advection-diffusion operator Eq. (20) equipped with no-flux boundary conditions on the entire solid boundary  $\Gamma \cup \tilde{\Gamma}$ .

By replacing  $\tilde{P}_{0,0}^{(0)}$  with  $w_0$  into Eq. (25) for the effective time-dependent velocities  $\mathcal{V}^i(t)$ , the asymptotic velocity components  $\mathcal{V}_\infty^i$  attain the form

$$\mathcal{V}_\infty^i = \int_{\Omega_f} J^i[w_0] d\xi = \int_{\Omega_f} (v^i w_0 - D^{ij} \partial_{\xi_j} w_0) d\xi \quad i = 1, 2. \quad (46)$$

Let us now analyze the asymptotic properties of the local moments  $P_{1,0}^{(1)}(\xi, t)$  and  $\tilde{P}_{1,0}^{(1)}(\tilde{\xi}, t)$ . By considering that

$$\lim_{t \rightarrow \infty} d_t M_{1,0}^{(1)}(t) \rightarrow \mathcal{V}_\infty^1 \Rightarrow \lim_{t \rightarrow \infty} M_{1,0}^{(1)}(t) \rightarrow \mathcal{V}_\infty^1 t + C_1, \quad (47)$$

the local moments  $P_{1,0}^{(1)}(\xi, t)$  and  $\tilde{P}_{1,0}^{(1)}(\tilde{\xi}, t)$  on long time scales can be expressed as follows:

$$\begin{aligned} \lim_{t \rightarrow \infty} P_{1,0}^{(1)}(\xi, t) &= w_0(\xi) [\mathcal{V}_\infty^1 t + b_{1,0}(\xi)], \\ \lim_{t \rightarrow \infty} \tilde{P}_{1,0}^{(1)}(\tilde{\xi}, t) &= \tilde{w}_0(\tilde{\xi}) [\mathcal{V}_\infty^1 t + \tilde{b}_{1,0}(\tilde{\xi})], \end{aligned} \quad (48)$$

where

$$\int_{\Omega_f} w_0(\xi) b_{1,0}(\xi) d\xi + \int_{\tilde{\Gamma}} \tilde{w}_0(\tilde{\xi}) \tilde{b}_{1,0}(\tilde{\xi}) d\tilde{\xi} = C_1. \quad (49)$$

By replacing Eq. (49) into the transport equations Eqs. (18)–(23) for local moments with  $q_1 = 1, q_2 = 0$ , one obtains that the stationary cell field  $w_0 b_{1,0}$  in the fluid phase satisfies the following transport equation and boundary conditions on the solid boundary,

$$\mathcal{L}_\xi[w_0 b_{1,0}] = w_0(\mathcal{V}_\infty^1 - v^1) + D^{1j} \partial_{\xi_j} w_0 + \partial_{\xi_j} (D^{1j} w_0), \quad (50)$$

$$\mathbf{J}[w_0 b_{1,0}] \cdot \mathbf{n}|_{\tilde{\xi}} = [-D^{1i} w_0 (\mathbf{e}_i \cdot \mathbf{n}) + \tilde{w}_0 \mathcal{V}_\infty^1]|_{\tilde{\xi}} \quad \forall \tilde{\xi} \in \tilde{\Gamma}, \quad (51)$$

$$\mathbf{J}[w_0 b_{1,0}] \cdot \mathbf{n}|_{\xi} = [-D^{1i} w_0 (\mathbf{e}_i \cdot \mathbf{n})]|_{\xi} \quad \forall \xi \in \Gamma, \quad (52)$$

and periodic boundary conditions on the edges of the periodicity cell not occupied by solid obstacles. Correspondingly, the stationary cell field  $\tilde{w}_0 \tilde{b}_{1,0}$  in the adsorbed phase satisfies the following equation:

$$(\tilde{w}_0 \tilde{b}_{1,0})|_{\tilde{\xi}} = \left[ \frac{k_a}{k_d} (w_0 b_{1,0}) - \frac{\tilde{w}_0}{k_d} \mathcal{V}_\infty^1 \right]|_{\tilde{\xi}} \quad \forall \tilde{\xi} \in \tilde{\Gamma}, \quad (53)$$

and the asymptotic effective dispersion entry  $\mathcal{D}_\infty^{1,1}$  attains the form

$$\begin{aligned} \mathcal{D}_\infty^{1,1} = & \int_{\Omega_f} D^{1,1} w_0 d\xi + \int_{\Omega_f} [(v^1 - \mathcal{V}_\infty^1)(w_0 b_{1,0}) \\ & - D^{1,j} \partial_{\xi_j} (w_0 b_{1,0})] d\xi - \mathcal{V}_\infty^1 \int_{\Gamma} (\tilde{w}_0 \tilde{b}_{1,0}) d\tilde{\xi}. \end{aligned} \quad (54)$$

Analogously, it can be shown that the asymptotic effective dispersion entries  $\mathcal{D}_\infty^{2,2}$  and  $\mathcal{D}_\infty^{1,2}$  attain the form

$$\begin{aligned} \mathcal{D}_\infty^{2,2} = & \int_{\Omega_f} D^{2,2} w_0 d\xi + \int_{\Omega_f} [(v^2 - \mathcal{V}_\infty^2)(w_0 b_{0,1}) \\ & - D^{2,j} \partial_{\xi_j} (w_0 b_{0,1})] d\xi - \mathcal{V}_\infty^2 \int_{\Gamma} (\tilde{w}_0 \tilde{b}_{0,1}) d\tilde{\xi}, \end{aligned} \quad (55)$$

$$\begin{aligned} \mathcal{D}_\infty^{1,2} = & \int_{\Omega_f} D^{1,2} w_0 d\xi + \frac{1}{2} \int_{\Omega_f} [(v^1 - \mathcal{V}_\infty^1)(w_0 b_{1,0}) \\ & - D^{1,j} \partial_{\xi_j} (w_0 b_{1,0}) + (v^2 - \mathcal{V}_\infty^2)(w_0 b_{0,1}) \\ & - D^{2,j} \partial_{\xi_j} (w_0 b_{0,1})] d\xi \\ & - \frac{1}{2} \int_{\Gamma} [\mathcal{V}_\infty^1 (\tilde{w}_0 \tilde{b}_{0,1}) + \mathcal{V}_\infty^2 (\tilde{w}_0 \tilde{b}_{1,0})] d\tilde{\xi}, \end{aligned} \quad (56)$$

where the stationary cell fields  $w_0 b_{0,1}$  and  $\tilde{w}_0 \tilde{b}_{0,1}$  satisfy the same Eqs. (51)–(54) as  $w_0 b_{1,0}$  and  $\tilde{w}_0 \tilde{b}_{1,0}$  where  $v^1$ ,  $\mathcal{V}_\infty^1$ , and  $D^{1,j}$  are replaced with  $v^2$ ,  $\mathcal{V}_\infty^2$ , and  $D^{2,j}$ , respectively.

These results coincide with that obtained by Brenner and Edwards<sup>19</sup> in the limiting case of infinitely fast adsorption/desorption process ( $k_d \rightarrow \infty$ ) and constant  $k_a/k_d$  adsorption/desorption rate ratio.

A similar approach can be adopted for the analysis of the asymptotic properties of the local second-order moments  $P_{2,0}^{(2)}(\xi, t)$  and  $\tilde{P}_{2,0}^{(2)}(\tilde{\xi}, t)$ . The starting point of the subsequent analysis is the following relationship between integral moments,

$$d_t M_{2,0}^{(2)} = d_t \sigma_{2,0}^2 + 2M_{1,0}^{(1)} d_t M_{1,0}^{(1)}, \quad (57)$$

that asymptotically can be expressed as follows:

$$\begin{aligned} \lim_{t \rightarrow \infty} d_t M_{2,0}^{(2)} = & 2\mathcal{D}_\infty^{1,1} + 2\mathcal{V}_\infty^1 \left( \int_{\Omega_f} P_{1,0}^{(1)}(\xi, t \rightarrow \infty) d\xi \right. \\ & \left. + \int_{\Gamma} \tilde{P}_{1,0}^{(1)}(\tilde{\xi}, t \rightarrow \infty) d\tilde{\xi} \right). \end{aligned} \quad (58)$$

By enforcing Eq. (48) for the asymptotic behavior of  $P_{1,0}^{(1)}(\xi, t)$  and  $\tilde{P}_{1,0}^{(1)}(\tilde{\xi}, t)$ , Eq. (58) can be rewritten as follows:

$$\begin{aligned} \lim_{t \rightarrow \infty} M_{2,0}^{(2)} = & 2\mathcal{D}_\infty^{1,1} t + (\mathcal{V}_\infty^1 t)^2 \\ & + 2\mathcal{V}_\infty^1 t \left( \int_{\Omega_f} w_0(\xi) b_0(\xi) d\xi + \int_{\Gamma} \tilde{w}_0(\tilde{\xi}) \tilde{b}_0(\tilde{\xi}) d\tilde{\xi} \right) + C_2, \end{aligned} \quad (59)$$

and therefore the second-order local moments  $P_{2,0}^{(2)}(\xi, t)$  and  $\tilde{P}_{2,0}^{(2)}(\tilde{\xi}, t)$  asymptotically can be expressed as follows:

$$\lim_{t \rightarrow \infty} P_{2,0}^{(2)}(\xi, t) = w_0(\xi) \left[ 2\mathcal{D}_\infty^{1,1} t + (\mathcal{V}_\infty^1 t)^2 + 2\mathcal{V}_\infty^1 b_{1,0}(\xi) t + c_{2,0}(\xi) \right], \quad (60)$$

$$\lim_{t \rightarrow \infty} \tilde{P}_{2,0}^{(2)}(\tilde{\xi}, t) = \tilde{w}_0(\tilde{\xi}) \left[ 2\mathcal{D}_\infty^{1,1} t + (\mathcal{V}_\infty^1 t)^2 + 2\mathcal{V}_\infty^1 \tilde{b}_{1,0}(\tilde{\xi}) t + \tilde{c}_{2,0}(\tilde{\xi}) \right], \quad (61)$$

where

$$\int_{\Omega_f} w_0(\xi) c_{2,0}(\xi) d\xi + \int_{\Gamma} \tilde{w}_0(\tilde{\xi}) \tilde{c}_{2,0}(\tilde{\xi}) d\tilde{\xi} = C_2. \quad (62)$$

By replacing Eqs. (60) and (61) into the transport equations Eqs. (18)–(23) for local moments with  $q_1 = 2, q_2 = 0$ , one obtains that the stationary cell field  $w_0 c_{2,0}$  in the fluid phase satisfies the following transport equation and boundary conditions on the solid boundary:

$$\begin{aligned} \mathcal{L}_\xi [w_0 c_{2,0}] = & 2w_0 b_{1,0} (\mathcal{V}_\infty^1 - v^1) + 2w_0 (\mathcal{D}_\infty^{1,1} - D^{1,1}) \\ & + 2D^{1,j} \partial_{\xi_j} (w_0 b_{1,0}) + 2\partial_{\xi_j} (D^{1,j} w_0 b_{1,0}) + 2D^{1,1} w_0, \end{aligned} \quad (63)$$

$$\begin{aligned} \mathbf{J}[w_0 c_{2,0}] \cdot \mathbf{n}|_{\tilde{\xi}} = & \left[ -D^{1,j} (w_0 b_{1,0}) (\mathbf{e}_i \cdot \mathbf{n}) + 2\tilde{w}_0 \tilde{b}_{1,0} \mathcal{V}_\infty^1 + 2\tilde{w}_0 \mathcal{D}_\infty^{1,1} \right] \Big|_{\tilde{\xi}} \\ & \forall \tilde{\xi} \in \Gamma, \end{aligned} \quad (64)$$

$$\mathbf{J}[w_0 c_{2,0}] \cdot \mathbf{n}|_{\tilde{\xi}} = -D^{1,j} (w_0 b_{1,0}) (\mathbf{e}_i \cdot \mathbf{n})|_{\tilde{\xi}} \quad \forall \tilde{\xi} \in \Gamma, \quad (65)$$

while the stationary cell field  $\tilde{w}_0 \tilde{c}_{2,0}$  in the adsorbed phase satisfies the following equation:

$$(\tilde{w}_0 \tilde{c}_{2,0})|_{\tilde{\xi}} = \left[ \frac{k_a}{k_d} (w_0 c_{2,0}) - 2 \frac{\tilde{w}_0 \tilde{b}_{1,0}}{k_d} \mathcal{V}_\infty^1 - 2 \frac{\tilde{w}_0}{k_d} \mathcal{D}_\infty^{1,1} \right] \Big|_{\tilde{\xi}} \quad \forall \tilde{\xi} \in \Gamma. \quad (66)$$

By replacing the asymptotic expressions Eqs. (48), (60), and (61) for first-order and second-order local moments into Eq. (32) for the centered third-order moments, the following compact expressions for  $d_t \mu_{3,0}$  and  $d_t \mu_{0,3}$  are obtained:

$$\begin{aligned} \lim_{t \rightarrow \infty} d_t \mu_{3,0}^{(3)} = & 3 \int_{\Omega_f} \left[ (v^1 - \mathcal{V}_\infty^1)(w_0 c_{2,0}) - D^{1,j} \partial_{\xi_j} (w_0 c_{2,0}) \right] d\xi \\ & + 6 \int_{\Omega_f} [(D^{1,1} - \mathcal{D}_\infty^{1,1})(w_0 b_{1,0})] d\xi \\ & - \int_{\Gamma} \left[ 3\mathcal{V}_\infty^1 (\tilde{w}_0 \tilde{c}_{2,0}) + 6\mathcal{D}_\infty^{1,1} (\tilde{w}_0 \tilde{b}_{1,0}) \right] d\tilde{\xi}, \end{aligned} \quad (67)$$

$$\begin{aligned} \lim_{t \rightarrow \infty} d_t \mu_{0,3}^{(3)} = & 3 \int_{\Omega_f} \left[ (v^2 - \mathcal{V}_\infty^2)(w_0 c_{0,2}) - D^{2,j} \partial_{\xi_j} (w_0 c_{0,2}) \right] d\xi \\ & + 6 \int_{\Omega_f} [(D^{2,2} - \mathcal{D}_\infty^{2,2})(w_0 b_{0,1})] d\xi \\ & - \int_{\Gamma} \left[ 3\mathcal{V}_\infty^2 (\tilde{w}_0 \tilde{c}_{0,2}) + 6\mathcal{D}_\infty^{2,2} (\tilde{w}_0 \tilde{b}_{0,1}) \right] d\tilde{\xi} =, \end{aligned} \quad (68)$$

where the stationary cell fields  $w_0 c_{0,2}$  and  $\tilde{w}_0 \tilde{c}_{0,2}$  satisfy the same Eqs. (63)–(66) as  $w_0 c_{2,0}$ , and  $\tilde{w}_0 \tilde{c}_{2,0}$  where  $v^1$ ,  $\mathcal{V}_\infty^1$ ,  $D^{1,j}$ ,  $w_0 b_{1,0}$ , and  $\tilde{w}_0 \tilde{b}_{1,0}$  are replaced with  $v^2$ ,  $\mathcal{V}_\infty^2$ ,  $D^{2,j}$ ,  $w_0 b_{0,1}$ , and  $\tilde{w}_0 \tilde{b}_{0,1}$ , respectively.

It can be observed that Eqs. (67) and (68) imply that both  $\mu_{3,0}^{(3)}$  and  $\mu_{0,3}^{(3)}$  in the long-time limit scale linearly with time,



$$\begin{aligned} \lim_{t \rightarrow \infty} d_t \mu_{3,0}^{(3)} = C_{3,0} &\Rightarrow \lim_{t \rightarrow \infty} \mu_{3,0}^{(3)} \sim C_{3,0} t, \\ \lim_{t \rightarrow \infty} d_t \mu_{0,3}^{(3)} = C_{0,3} &\Rightarrow \lim_{t \rightarrow \infty} \mu_{0,3}^{(3)} \sim C_{0,3} t. \end{aligned} \tag{69}$$

Since also the variances  $\sigma_{2,0}^2$  and  $\sigma_{0,2}^2$  scale linearly asymptotically

$$\lim_{t \rightarrow \infty} \sigma_{2,0}^2 \sim 2 \mathcal{D}_{\infty}^{1,1} t, \quad \lim_{t \rightarrow \infty} \sigma_{0,2}^2 \sim 2 \mathcal{D}_{\infty}^{2,2} t, \tag{70}$$

then the time-dependent skewnesses  $sk^{(1,1)}(t)$  and  $sk^{(2,2)}(t)$  asymptotically decay to zero as

$$\lim_{t \rightarrow \infty} sk^{(1,1)} \sim \frac{C_{3,0}}{(2\mathcal{D}_{\infty}^{1,1})^{3/2}} t^{-1/2}, \quad \lim_{t \rightarrow \infty} sk^{(2,2)} \sim \frac{C_{0,3}}{(2\mathcal{D}_{\infty}^{2,2})^{3/2}} t^{-1/2}. \tag{71}$$

It is worth noting that the stationary cell fields  $b_{1,0}$  and  $\tilde{b}_{1,0}$  are both defined modulo an additive constant. Indeed, if  $w_0 b_{1,0}$  and  $\tilde{w}_0 \tilde{b}_{1,0}$  are solutions of Eqs. (50)–(53), then also  $w_0 b_{1,0} + C w_0$  and  $\tilde{w}_0 \tilde{b}_{1,0} + C \tilde{w}_0$  are solutions of the same set of equations,  $C$  being a constant, the same for both fields. However, the contribution of the additive term is immaterial for the estimate of the effective asymptotic dispersion tensor  $\mathcal{D}_{\infty}^{ij}$ . By way of example, by replacing  $w_0 b_{1,0} + C w_0$  and  $\tilde{w}_0 \tilde{b}_{1,0} + C \tilde{w}_0$  into Eq. (54) for  $\mathcal{D}_{\infty}^{1,1}$  one obtains an extra term,

$$\begin{aligned} C \int_{\Omega_f} [(v^1 - \mathcal{V}_{\infty}^1) w_0 - D^{1j} \partial_{\xi_j} (w_0)] d\xi - C \mathcal{V}_{\infty}^1 \int_{\tilde{\Gamma}} \tilde{w}_0 d\tilde{\xi} \\ = C \mathcal{V}_{\infty}^1 \left( 1 - \int_{\Omega_f} w_0 d\xi - \int_{\tilde{\Gamma}} \tilde{w}_0 d\tilde{\xi} \right) = 0, \end{aligned} \tag{72}$$

that is zero because of the normalization of the cell equilibrium distribution.

The same can be said for the stationary cell fields  $c_{2,0}$  and  $\tilde{c}_{2,0}$ , solutions of Eqs. (63)–(66), defined up to an additive constant, the same for both fields, the choice of which has no influence on the estimate of the centered third-order moment Eq. (67).

### A. Asymptotic analysis for a uniform Frobenius eigenfunction $w_0$

The time-dependent and asymptotic formulations of the transport problem, developed in Secs. II A–III, have a general validity. The asymptotic analysis developed in this section is limited to the case of no-slip boundary conditions for the fluid velocity field.

When the normal components of the velocity field vanish at all the solid boundaries  $\mathbf{v} \cdot \mathbf{n}|_{\tilde{\xi}} = 0 \forall \tilde{\xi} \in \Gamma \cup \tilde{\Gamma}$ , the Frobenius eigenfunction  $w_0(\xi)$  is uniform on  $\Omega_f$ , i.e.,  $w_0(\xi) = w_0 = \text{constant}$ . Therefore, by enforcing Eq. (46) and the integral constrain  $M_{0,0}^{(0)}(t) = 1$  (valid at any time instant  $t$ ), the following expressions for  $w_0$  and  $\tilde{w}_0(\tilde{\xi})$  hold true:

$$w_0 = \frac{1}{V_f} \frac{1}{(1+K)}, \quad \tilde{w}_0(\tilde{\xi}) = \frac{k_a(\tilde{\xi})}{k_d(\tilde{\xi})} w_0, \tag{73}$$

where  $V_f = \text{meas}(\Omega_f)$  is the measure (volume or area) of the fluid phase,  $\tilde{S} = \text{meas}(\tilde{\Gamma})$  is the measure (area or length) of the adsorbing boundary and  $K$  is the average retention factor

$$K = \frac{\tilde{S}}{V_f} \left\langle \frac{k_a}{k_d} \right\rangle_{\tilde{\Gamma}}, \quad \left\langle \frac{k_a}{k_d} \right\rangle_{\tilde{\Gamma}} = \frac{1}{\tilde{S}} \int_{\tilde{\Gamma}} \frac{k_a(\tilde{\xi})}{k_d(\tilde{\xi})} d\tilde{\xi}. \tag{74}$$

Moreover, since  $w_0$  is uniform on  $\Omega_f$  all the spatial derivatives of  $w_0$  are zero and the effective asymptotic velocity components attain the form

$$\mathcal{V}_{\infty}^i = \omega_0 \int_{\Omega_f} v^i(\xi) d\xi = \frac{1}{(1+K)} \left( \frac{1}{V_f} \int_{\Omega_f} v^i(\xi) d\xi \right) = \frac{1}{(1+K)} \langle v^i \rangle_{\Omega_f}, \tag{75}$$

representing the fluid velocity components  $v^i$ , averaged over the fluid volume of the unit cell and weighed with respect to the fraction of solute particles in the mobile phase,  $c_0 = \int_{\Omega_f} w_0 d\xi = (1+K)^{-1}$ .

By enforcing the further assumption of a uniform solute diffusivity, i.e.,  $D^{i,i}(\xi) = D = \text{constant}$ ,  $D^{ij} = 0$  for  $i \neq j$ , the transport equations (50)–(53) for the stationary b-field  $b_{1,0}$  simplify to

$$\mathcal{L}_{\xi}[b_{1,0}] = (\mathcal{V}_{\infty}^1 - v^1), \tag{76}$$

$$-D \nabla b_{1,0} \cdot \mathbf{n}|_{\tilde{\xi}} = \left[ -D (\mathbf{e}_1 \cdot \mathbf{n}) + \mathcal{V}_{\infty}^1 \frac{k_a}{k_d} \right]_{\tilde{\xi}} \quad \forall \tilde{\xi} \in \tilde{\Gamma}, \tag{77}$$

$$-D \nabla b_{1,0} \cdot \mathbf{n}|_{\xi} = -D (\mathbf{e}_1 \cdot \mathbf{n})|_{\xi} \quad \forall \xi \in \Gamma, \tag{78}$$

$$(\tilde{b}_{1,0})|_{\tilde{\xi}} = \left[ (b_{1,0}) - \frac{\mathcal{V}_{\infty}^1}{k_d} \right]_{\tilde{\xi}} \quad \forall \tilde{\xi} \in \tilde{\Gamma}, \tag{79}$$

and the asymptotic dispersion entry  $\mathcal{D}_{\infty}^{1,1}$  attains the form

$$\begin{aligned} \mathcal{D}_{\infty}^{1,1} = \frac{D}{1+K} + \frac{1}{1+K} \langle (v^1 - \mathcal{V}_{\infty}^1) b_{1,0} - D \partial_{\xi,1} (b_{1,0}) \rangle_{\Omega_f} \\ - \frac{\mathcal{V}_{\infty}^1}{1+K} \left\langle \left( \frac{k_a}{k_d} \frac{\tilde{S}}{V_f} \right) b_{1,0} \Big|_{\tilde{\Gamma}} \right\rangle + \frac{(\mathcal{V}_{\infty}^1)^2}{1+K} \left\langle \left( \frac{k_a}{k_d} \frac{\tilde{S}}{V_f} \right) \frac{1}{k_d} \right\rangle_{\tilde{\Gamma}}. \end{aligned} \tag{80}$$

In the case of  $k_a(\tilde{\xi})$  and  $k_d(\tilde{\xi})$  attain constant values on  $\tilde{\Gamma}$ , i.e.,  $k_a(\tilde{\xi}) = k_a = \text{constant}$  and  $k_d(\tilde{\xi}) = k_d = \text{constant}$ , Eq. (80) simplifies to

$$\begin{aligned} \mathcal{D}_{\infty}^{1,1} = \frac{D}{1+K} + \frac{1}{1+K} \langle (v^1 - \mathcal{V}_{\infty}^1) b_{1,0} - D \partial_{\xi,1} (b_{1,0}) \rangle_{\Omega_f} \\ - \mathcal{V}_{\infty}^1 \frac{K}{1+K} \langle b_{1,0} \Big|_{\tilde{\Gamma}} \rangle_{\tilde{\Gamma}} + (\mathcal{V}_{\infty}^1)^2 \frac{K}{1+K} \frac{1}{k_d}. \end{aligned} \tag{81}$$

The last term of the right-hand side of Eqs. (80) and (81) vanishes in the limiting case of infinitely fast adsorption/desorption process in which case  $k_d \rightarrow \infty$  while the retention factor  $K$  assumes a finite value anyway. The corresponding expressions for  $\mathcal{D}_{\infty}^{2,2}$  and  $\mathcal{D}_{\infty}^{1,2}$  can be easily deduced from Eq. (81) and are not reported here for sake of brevity.

It is worth noting that Eq. (81) for  $\mathcal{D}_{\infty}^{1,1}$  coincides with that obtained by Yan *et al.*<sup>30</sup> [Eq. (30) in their paper] by the method of volume averaging, by simply enforcing the following correspondences  $k_a/k_d = \gamma\delta$ ,  $k_d = k/\delta$ ,  $\mathbf{f} = (b_{1,0}, b_{0,1})$  and setting to zero the arbitrary constant  $C_1$  entering the integral constrain Eq. (49).

### IV. CASE STUDY I: THE SINUSOIDAL CHANNEL

We analyze the temporal evolution of dispersion properties of a single solute in a sinusoidal tube in the presence of a steady-state pressure-driven incompressible Stokes flow with no-slip boundary conditions at the tube wall coated with a thin adsorbing layer characterized

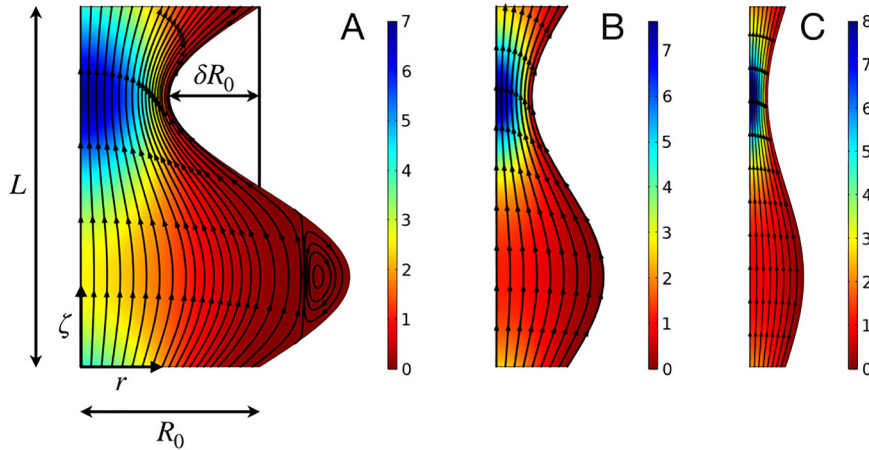


**FIG. 2.** Streamlines of the velocity field in the sinusoidal unit cell for  $\delta = 0.5$  and  $\lambda = L/R_0 = 2, 5,$  and  $10$ . Colors indicate the intensity of the axial velocity component  $v^z/W$ ,  $W$  being the average axial velocity at the inlet section  $\zeta = 0$  of the unit cell  $\Omega$ . Panel (a)  $\lambda = 2$ ; panel (b)  $\lambda = 5$ ; and panel (c)  $\lambda = 10$ .

by uniform adsorption  $k_a$  (m/s) and desorption  $k_d$  (1/s) kinetic constants. The solute diffusivity  $D$  is also assumed uniform in the fluid domain and negligible in the adsorbed phase (no surface diffusion).

The sinusoidal channel with average radius  $R_0$ , wavelength  $L$  and wave amplitude  $\delta R_0$  can be viewed as the periodic repetition, along the axial coordinate  $z$ , of a periodicity cell  $\Omega$  of length  $L$ ,

$$\Omega = \{(r, \zeta, \theta) \mid 0 \leq r \leq R(\zeta), 0 \leq \zeta \leq L, 0 \leq \theta < 2\pi\}, \quad (82)$$

$$R(\zeta) = R_0 + (\delta R_0) \sin(2\pi\zeta/L),$$

because the global axial coordinate  $z$  can be expressed as  $z = mL + \zeta$  where  $m$  is the unit cell number and  $\zeta \in [0, L)$  the local coordinate. For this axially periodic medium, the fluid phase  $\Omega_f$  coincides with  $\Omega$  and  $\Gamma = \emptyset$  because the solid non-porous adsorbing phase  $\tilde{\Gamma}$  is the entire tube wall  $\tilde{\Gamma} = \{(r, \zeta, \theta) \mid r = R(\zeta), 0 \leq \zeta \leq L, 0 \leq \theta < 2\pi\}$ .

The inlet condition analyzed is an impulsive injection of solute uniformly distributed over the inlet cross section. This axisymmetric inlet condition and the uniformity of the adsorption and desorption kinetic constants simplify the dispersion problem to a 2d axisymmetric transport problem, in which the particle density functions, and thus also the local moments, are independent of the angular coordinate  $\theta$ .

For a fixed value of the dimensionless wave amplitude  $\delta$ , the velocity field changes significantly with the dimensionless wavelength  $\lambda = L/R_0$ . Figure 2 shows the behavior of the streamlines for  $\delta = 0.5$ ,  $\lambda = 2, 5,$  and  $10$  and the intensity of the axial velocity component  $v^z/W$ ,  $W$  being the reference velocity chosen as the average axial velocity at the inlet section  $\zeta = 0$  of the unit cell. It can be observed that for  $\lambda < 3$  a large recirculation zone appears in the region of the maximum cross section enlargement. Also, the surface-over-volume ratio  $\tilde{S}/V$  changes with  $\lambda$ , attaining decreasing values as  $\lambda$  increases, namely  $\tilde{S}R_0/V \simeq 2.603, 1.942,$  and  $1.821$  for  $\lambda = 2, 5,$  and  $10$ , respectively.

For this axial-symmetric channel possessing axial spatial periodicity, one is interested in evaluating the transient behavior (and the asymptotic values) of the effective axial velocity  $\mathcal{V}^z(t)$ , the axial dispersion coefficient  $\mathcal{D}^z(t)$  and the skewness  $sk^z(t)$  of the marginal pdf  $F_z(z, t)$ ,  $F_z(z, t) dz$  representing the fraction of solute particles (in both the mobile and adsorbed phase) falling in the range  $(z, z + dz)$ , regardless of the radial ( $r$ ) and angular ( $\theta$ ) solute particle position. The evaluation of these quantities requires the estimate of the space-time

evolution of the local moments  $P^{(q)}$  and  $\tilde{P}^{(q)}$  where the simplified notation  $P^{(q)} = P_{q,0}^{(q)}$  and  $\tilde{P}^{(q)} = \tilde{P}_{q,0}^{(q)}$ ,  $M^{(q)} = M_{q,0}^{(q)}$ ,  $m^{(q)} = m_{q,0}^{(q)}$ ,  $\tilde{m}^{(q)} = \tilde{m}_{q,0}^{(q)}$ , and  $\sigma^2 = \sigma_{2,0}^2$  has been adopted because  $q_2 = 0$  and  $q = q_1 + q_2 = q_1$  since only axial periodicity can be enforced, i.e.,  $\mathbf{m} = m^1$ ,  $\boldsymbol{\xi} = \boldsymbol{\xi}^1 = \boldsymbol{\zeta}$ . Correspondingly, the effective axial transport parameters can be identified as  $\mathcal{V}^z(t) = \mathcal{V}^1(t)$ ,  $\mathcal{D}^z(t) = \mathcal{D}^{1,1}(t)$ , and  $sk^z(t) = sk^{1,1}(t)$  with respect to the notation adopted in Sec. II.

The initial condition investigated is that of a uniform impulsive solute distribution at the inlet section, i.e.,  $p(r, \theta, z, 0) = \delta(z)/(\pi R_0^2)$ ,  $\tilde{p}(R(z), \theta, z) = 0$ , that for the local moments implies  $P^{(0)}(r, \theta, \zeta) = \delta(\zeta)/(\pi R_0^2)$ ,  $P^{(q)}(r, \theta, \zeta) = 0$  for  $q > 0$  and  $\tilde{P}^{(q)}(R(\zeta), \theta, \zeta) = 0$  for  $q \geq 0$ . For this initial condition, as for any initial condition that does not depend on the angular coordinate  $\theta$ , all the local moments in both the mobile and adsorbed phase do not depend on  $\theta$ , i.e.,  $P^{(q)}(\boldsymbol{\chi}, t) = P^{(q)}(r, \zeta, t)$  and  $\tilde{P}^{(q)}(\tilde{\boldsymbol{\chi}}, t) = \tilde{P}^{(q)}(R(\zeta), \zeta, t)$ .

The transport equations and boundary conditions for the hierarchy of local moments can be easily deduced from Eqs. (18)–(23) by setting  $q_1 = q$ ,  $q_2 = 0$ ,  $\mathbf{e}_1 = \mathbf{e}_z$ ,  $(v^1, v^2) = (v^z, v^r)$ ,  $D^{1,1} = D^{2,2} = D$ ,  $D^{1,2} = D^{2,1} = 0$ , thus obtaining

$$\partial_t P^{(q)}(\boldsymbol{\chi}, t) = \mathcal{L}_{\zeta,r}^{(q)}[P^{(q)}] + q \left[ v^z P^{(q-1)} - 2D \partial_\zeta (P^{(q-1)}) \right] + q(q-1)P^{(q-2)} \quad \forall \boldsymbol{\chi} \in \Omega_f, \quad (83)$$

$$\mathbf{J}[P^{(q)}] \cdot \mathbf{n}|_{\tilde{\Gamma}} = -qD P^{(q-1)}(\mathbf{e}_z \cdot \mathbf{n})|_{\tilde{\Gamma}} + k_a P^{(q)}(\tilde{\boldsymbol{\chi}}, t) - k_d \tilde{P}^{(q)}(\tilde{\boldsymbol{\chi}}, t), \quad \forall \tilde{\boldsymbol{\chi}} \in \tilde{\Gamma}, \quad (84)$$

$$\partial_t \tilde{P}^{(q)}(\tilde{\boldsymbol{\chi}}, t) = k_a P^{(q)}(\tilde{\boldsymbol{\chi}}, t) - k_d \tilde{P}^{(q)}(\tilde{\boldsymbol{\chi}}, t) \quad \forall \tilde{\boldsymbol{\chi}} \in \tilde{\Gamma}, \quad (85)$$

where  $\mathbf{J}[\cdot] = (J^z[\cdot], J^r[\cdot])$  and  $\mathcal{L}_{\zeta,r}^{(q)}[\cdot]$  are the flux operator and the cell advection-diffusion operator in cylindrical coordinates, respectively,

$$\mathbf{J}[P^{(q)}] = J^r[P^{(q)}]\mathbf{e}_r + J^z[P^{(q)}]\mathbf{e}_z = [v^r P^{(q)} - D \partial_r P^{(q)}]\mathbf{e}_r + [v^z P^{(q)} - D \partial_\zeta P^{(q)}]\mathbf{e}_z, \quad (86)$$

$$\mathcal{L}_{\zeta,r}^{(q)}[P^{(q)}] = -\nabla \cdot \mathbf{J}[P^{(q)}] = -r^{-1} \partial_r (r J^r[P^{(q)}]) + \partial_\zeta J^z[P^{(q)}]. \quad (87)$$

According to Eq. (25), the effective time-dependent axial velocity  $\mathcal{V}^z(t)$  can be computed as follows:

$$\begin{aligned} \mathcal{V}^z(t) &= \int_{\Omega_f} J^z[P^{(0)}] d\chi = \int_0^L d\zeta \int_0^{R(\zeta)} J^z[P^{(0)}] 2\pi r dr \\ &= \int_{\Omega_f} (v^z P^{(0)} - D\partial_\zeta(P^{(0)})) d\chi, \end{aligned} \quad (88)$$

converging asymptotically to  $\mathcal{V}^z_\infty$ , Eq. (75)

$$\mathcal{V}^z_\infty = \frac{1}{1+K} \langle v^z \rangle_{\Omega_f} = \frac{1}{1+K} \frac{W}{1+\delta^2/2}, \quad K = \frac{\tilde{S}}{V_f} \frac{k_a}{k_b}. \quad (89)$$

$\langle v^z \rangle_{\Omega_f} = W/(1 + \delta^2/2)$  is the seepage fluid velocity.

According to Eq. (29), the effective time-dependent axial dispersion coefficient  $\mathcal{D}^z(t)$  can be computed as follows:

$$\begin{aligned} \mathcal{D}^z(t) &= D \int_{\Omega_f} P^{(0)} d\chi + \int_{\Omega_f} [(v^z - \mathcal{V}^z)P^{(1)} - D\partial_\zeta P^{(1)}] d\chi \\ &\quad - \mathcal{V}^z \int_{\Gamma} \tilde{P}^{(1)} d\tilde{\chi}, \end{aligned} \quad (90)$$

converging asymptotically to  $\mathcal{D}^z_\infty$  whose expression coincides with that of  $\mathcal{D}^{z,1}_\infty$ , Eq. (81) by identifying  $v^1$ ,  $\mathcal{V}^1_\infty$ , and  $\partial_{\xi,1}$  with  $v^z$ ,  $\mathcal{V}^z_\infty$ , and  $\partial_\zeta$ . Finally, the axial skewness  $sk^z(t)$  can be computed as follows:

$$sk^z(t) = \frac{\int_0^t d_t \mu_3^z(t') dt'}{\left( \int_0^t 2\mathcal{D}^z(t') dt' \right)^{3/2}}, \quad (91)$$

where

$$\begin{aligned} d_t \mu_3^z(t) &= 3 \int_{\Omega_f} [(v^z - \mathcal{V}^z)P^{(2)} - D\partial_\zeta P^{(2)}] d\chi \\ &\quad + 6(D - \mathcal{D}^z) \int_{\Omega_f} P^{(1)} d\chi \\ &\quad - \int_{\Gamma} [3\mathcal{V}^z \tilde{P}^{(2)} + 6\mathcal{D}^z \tilde{P}^{(1)}] d\tilde{\chi}. \end{aligned} \quad (92)$$

Alternatively, the skewness can be computed directly from its definition Eq. (13) by computing first-, second-, and third-order integral moments, the latter requiring the estimate of third-order local moments  $P^{(3)}$  and  $\tilde{P}^{(3)}$ .

### A. Asymptotic analysis

Preliminarily, asymptotic dispersion properties are analyzed as a function of the dimensionless parameters, namely the cross-sectional Peclet number  $Pe$ , the adsorption/desorption Damköhler numbers  $Da_a$  and  $Da_d$ , the equilibrium constant  $\gamma$  and the retention factor  $K$ , defined as follows:

$$\begin{aligned} Pe &= \frac{W_r L_r}{D}, \quad Da_a = \frac{k_a L_r}{D}, \quad Da_d = \frac{k_d L_r^2}{D}, \\ \gamma &= \frac{Da_a}{Da_d}, \quad K = \frac{k_a \tilde{S}}{k_d V_f} = \gamma \frac{\tilde{S} L_r}{V_f}, \end{aligned} \quad (93)$$

where the reference length  $L_r$  has been chosen as the tube radius at the inlet section  $\zeta = 0$ ,  $r = R_0$  and the reference velocity  $W_r$  is the average fluid velocity at the inlet section  $W$ .

Figure 3 shows the behavior of the normalized effective axial velocity  $\mathcal{V}^z_\infty/W$ , evaluated from Eq. (89), as a function of the equilibrium constant  $\gamma$  for a straight tube  $\delta = 0$ , and for three different sinusoidal channels with the same  $\delta = 0.5$  and different values of the dimensionless wavelength  $\lambda = 2, 5, \text{ and } 10$  (same as shown in Fig. 2). The sinusoidal tubes and the straight channel are characterized by the same inlet average velocity  $W$  and therefore by different seepage velocities  $\langle v^z \rangle_{\Omega_f}$ , Eq. (89). The sigmoidal curve  $\mathcal{V}^z_\infty/W$  vs  $\gamma$  exhibits the two expected limit values, i.e.,  $\mathcal{V}^z_\infty \rightarrow \langle v^z \rangle_{\Omega_f}$  for  $\gamma \rightarrow 0$  and  $\mathcal{V}^z_\infty \rightarrow 0$  for  $\gamma \rightarrow \infty$ . These results are independent of the Peclet value and unaffected by the presence of a large recirculation/stagnant zone for small wavelengths, e.g.,  $\lambda = 2$ . Indeed, differences between curves, corresponding to different values of  $\lambda$ , are uniquely due to different surface-to-volume ratios  $\tilde{S}/V$  because the three sinusoidal channels are characterized by the same wave amplitude  $\delta$  and therefore the same seepage velocity  $\langle v^z \rangle_{\Omega_f}$ .

On the contrary, the Peclet value as well as the wavelength  $\lambda$  strongly influences the effective asymptotic dispersion coefficient  $\mathcal{D}^z_\infty$  as shown in Fig. 4 where the dimensionless height equivalent of a theoretical plate  $HETP^*$ ,

$$HETP^* = \frac{HETP}{R_0} = \frac{\mathcal{D}^z_\infty}{R_0 \mathcal{V}^z_\infty} = \frac{(\mathcal{D}^z_\infty/D)}{Pe (\mathcal{V}^z_\infty/W)}, \quad (94)$$

is shown as a function of  $Pe$  (Van Deemter plot<sup>82,83</sup>) for a straight tube and for two different sinusoidal channels with  $\lambda = 2, 10$ . Specifically, Fig. 4(a) shows the Van Deemter plots for  $\gamma = 0$ , i.e., in the absence of the adsorbing surface while Figs. 4(b)–4(d) show the same curves for  $\gamma = 1$  and for different values of  $Da_d$ , namely  $Da_d = Da_a = 0.1, 1, \text{ and } 100$ .

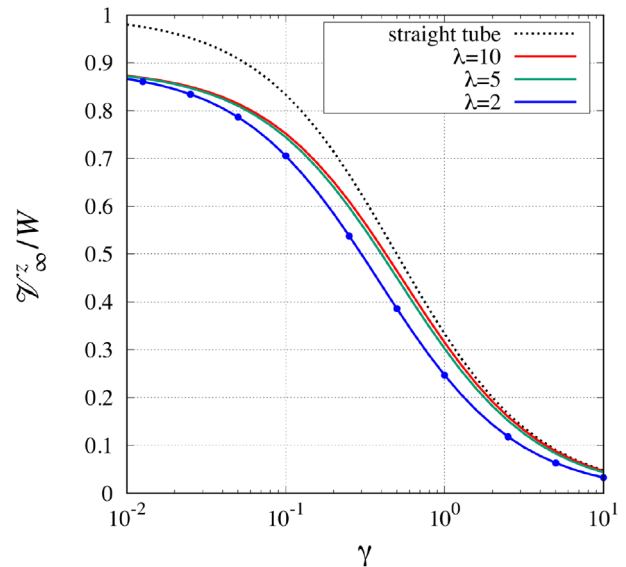
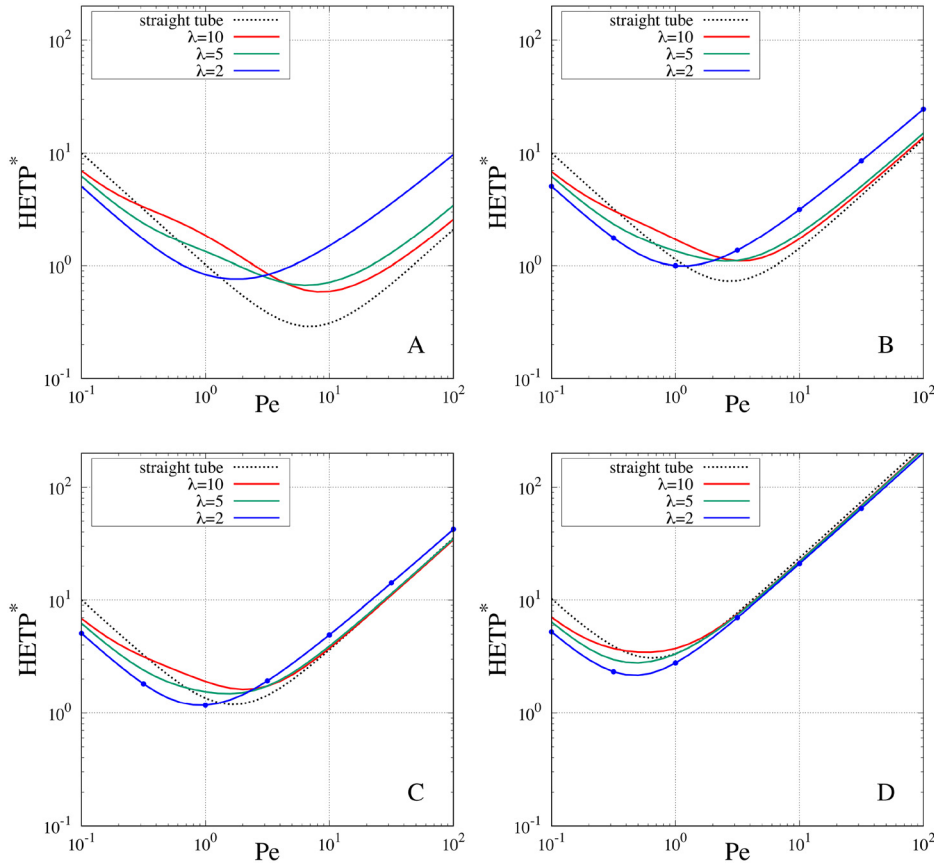


FIG. 3. Normalized asymptotic effective axial velocity  $\mathcal{V}^z_\infty/W$ , Eq. (90), vs the equilibrium constant  $\gamma = Da_a/Da_d$  for a straight cylindrical channel (dotted curve) and for three different sinusoidal channels with  $\delta = 0.5$  and  $\lambda = 2, 5, \text{ and } 10$ . Blue points are the result obtained from the asymptotic scaling  $M_{1,0}^{(1)} \sim \mathcal{V}^z_\infty t$ .



**FIG. 4.**  $HETP^*$  vs  $Pe$  for a straight tube (dotted curves) and for three different sinusoidal channels with  $\delta=0.5$  and  $\lambda=2, 5$ , and  $10$ . Panel (a)  $\gamma=0$ , no adsorption. Panel (b)  $\gamma=1$ ,  $Da_a = Da_d = 100$  (infinitely fast adsorption/desorption process). Panel (c)  $\gamma=1$ ,  $Da_a = Da_d = 1$  (adsorption/desorption time scale comparable to diffusion time scale). Panel (d)  $\gamma=1$ ,  $Da_a = Da_d = 0.1$  (adsorption/desorption process slower than radial diffusion). Blue points are the result obtained from the asymptotic scaling  $\sigma_{2,0}^2 \sim 2\mathcal{D}_\infty^z t$ .

Focusing on the convection-enhanced regime ( $Pe \geq 10$ ), Fig. 4(a) clearly shows that, in the absence of adsorption, the  $HETP^*$  increases significantly as  $\lambda$  decreases. The same phenomenon can be observed in the presence of adsorption [see Figs. 4(b)–4(d)] when the adsorption/desorption process is faster than radial diffusion,  $Da_a = Da_d = 100$ . The effect of wall curvature becomes less and less significant as the Damköhler numbers decrease. Indeed, for  $Da_a = Da_d = 0.1$  the adsorption/desorption process is slower than radial diffusion and becomes the controlling step. As a consequence, the  $HETP^*$  curves move toward higher values and become almost independent of the wavelength  $\lambda$ .

It must be observed that asymptotic effective parameters  $\mathcal{V}_\infty^z$  and  $\mathcal{D}_\infty^z$ , reported in Figs. 3 and 4, are obtained from the asymptotic analysis developed in Sec. III A, in agreement with long-range/large-distance theoretical results developed *in primis* by Brenner and Edwards<sup>19</sup> for  $Da_d \rightarrow \infty$ , and subsequently by Yan *et al.*<sup>30</sup> for any finite value of  $Da_d$ . These data can be used to check the validity and reliability of the transient analysis of macrotransport parameters developed in Sec. II A and here adapted to the case of the axial-symmetric axial-periodic sinusoidal channel, Eqs. (84)–(93). Indeed, blue points in Figs. 3 and 4 are the results for  $\mathcal{V}_\infty^z/W$  and for  $HETP^*$  obtained via the numerical integration of Eqs. (84)–(86) for the hierarchy of time-dependent local moments  $P^{(q)}(\chi, t)$ , subsequently evaluating the asymptotic scalings  $M_{1,0}^{(1)} \sim \mathcal{V}_\infty^z t$  and  $\sigma_{2,0}^2 \sim 2\mathcal{D}_\infty^z t$  as shown in Fig. 5 for  $\lambda = 10$ ,  $\gamma = 1$ ,  $Pe = 100$  and different values of  $Da_d$ , namely

$Da_d = Da_a = 0.05, 0.1, 1$ , and  $100$ . The excellent agreement between the results obtained from the asymptotic analysis (based on the stationary cell field  $b_{1,0}$ ) and the asymptotic behavior of the transient analysis based on exact local moments, is a confirmation of the reliability of the whole theoretical framework.

## B. Transient analysis

The transient analysis is extremely important as it reveals some important features of the dispersion process that are not evident or cannot be captured by the asymptotic analysis. Figure 6 shows the transient behavior for  $Pe=100$  of the normalized axial velocity  $\mathcal{V}^z(\tau)/W$ , the normalized dispersion coefficient  $\mathcal{D}^z(\tau)/D$ , the dispersion coefficient rescaled onto its asymptotic value  $\mathcal{D}^z(\tau)/\mathcal{D}_\infty^z$  and the skewness  $sk^z(\tau)$  for a straight tube and for two different sinusoidal channels, one with a large and one with a small wavelength  $\lambda$ . The unitary equilibrium constant  $\gamma=1$  implies that  $Da_a = Da_d$ , i.e., the adsorption and desorption processes occur on the same time scales and the parameter  $Da_d$  dictates the rate-controlling step between adsorption/desorption and radial diffusion for  $Pe > 10$  (convection-enhanced regime).

From the analysis of Fig. 6, many significant observations can be derived that contribute to a deeper understanding of the physics of the dispersion process in the presence of adsorption

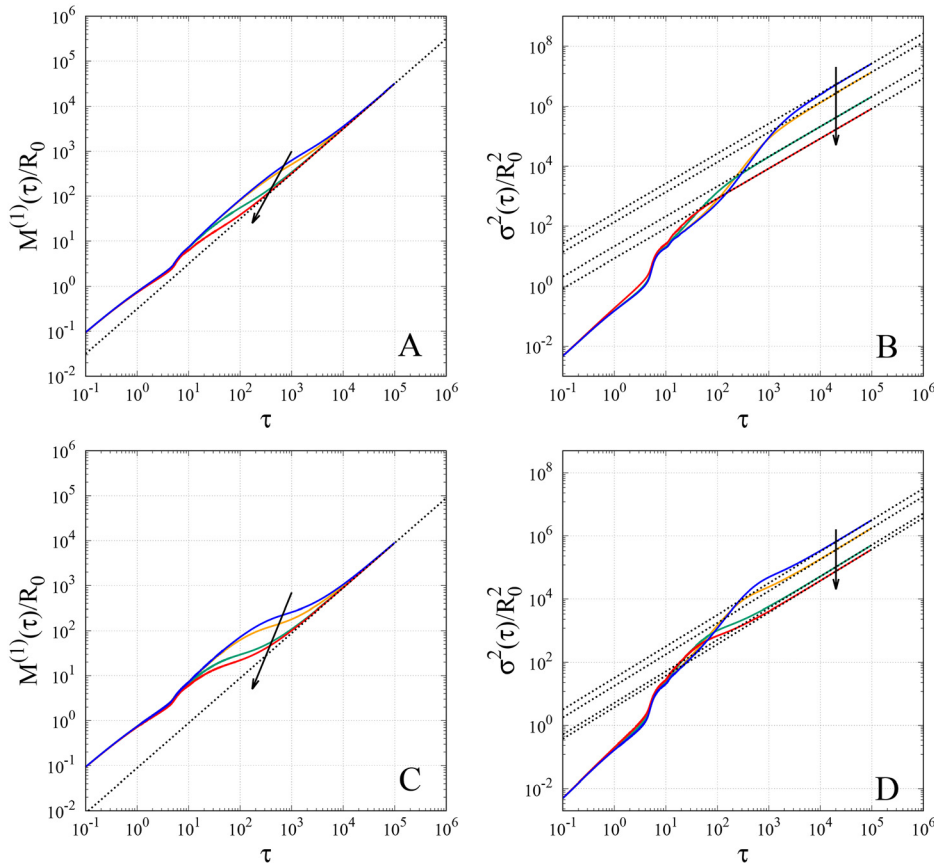


**FIG. 5.** Transient behavior of  $M^{(1)}(\tau)$  [panels (a) and (c)] and  $\sigma^2(\tau)$  [panels (b) and (d)] at  $Pe=100$  for a sinusoidal channel with  $\delta=0.5$ ,  $\lambda=10$ . Different curves correspond to different values of  $Da_d = 0.05, 0.1, 1$ , and  $100$ , while  $Da_a = \gamma Da_d$ . Arrows indicate increasing values of  $Da_d$ . Dashed lines highlight the asymptotic linear behaviors  $M^{(1)}/R_0 \sim (\mathcal{V}_\infty^z/W)\tau$  and  $\sigma^2/R_0^2 \sim 2(\mathcal{D}_\infty^z/D)\tau/Pe$ ,  $\tau = tW/R_0$  being the dimensionless time. Panels (a) and (b):  $\gamma=1$ ; panels (c) and (d):  $\gamma=5$ .

1. For both straight and sinusoidal channels, the effective velocity  $\mathcal{V}^z$  and the effective dispersion coefficient  $\mathcal{D}^z$  converge toward asymptotic constant values  $\mathcal{V}_\infty^z$  and  $\mathcal{D}_\infty^z$  on the same dimensionless time scale  $\tau^*$ , namely  $\tau^* \simeq Pe/Da_d$  for  $Da_d < 1$  (adsorption/desorption controlled process) and  $\tau^* \simeq Pe$  for  $Da_d > 1$  (diffusion-controlled). On the contrary, a significant skewness ( $sk^z > 0.1$ ) of the marginal pdf  $F_z(z, t)$  is still present, for all the  $Da_d$  values investigated, on a time scale  $\tau^*$  order of  $10^4$ , i.e., two orders of magnitude larger than the  $Pe$  value. Indeed, only after  $\mathcal{V}^z$  and  $\mathcal{D}^z$  attained the asymptotic values, the marginal pdf  $F_z$  becomes unimodal and the skewness  $sk^z$  starts to decay by settling onto the asymptotic  $\tau^{-1/2}$  branch. Therefore, the time scale for achieving the macro-transport regime, described by the macro-transport equation Eq. (7) that implies a Gaussian (symmetric) marginal pdf, is largely underestimated if one bases the analysis on the attainment of a constant velocity  $\mathcal{V}_\infty^z$  or a constant dispersion coefficient  $\mathcal{D}_\infty^z$ .
2. The adsorption process strongly amplifies the phenomenon of the overshoot for the effective dispersion coefficient  $\mathcal{D}^z$  that, on short/intermediate time scales, reaches values greater than asymptotic one  $\mathcal{D}_\infty^z$ . This phenomenon has been already observed, in a much weaker form, by Vedel *et al.*,<sup>76</sup> Vedel and Bruus,<sup>84</sup> and Adrover *et al.*<sup>25</sup> in straight and sinusoidal channels for a pointwise initial condition in the absence of wall adsorption. In the presence of wall adsorption, the

phenomenon of the overshoot is enormously amplified, especially for large values of  $Da_d$  that imply a fast adsorption process and therefore a fast depletion of solute particles from the slow-moving fluid near the adsorbing walls. This peculiar feature of the dispersion coefficient in the presence of adsorption has been already highlighted by Zhang *et al.*<sup>29</sup> in dealing with a two-dimensional straight channel with parallel adsorbing/desorbing walls. The transient formulation developed in Sec. II A permits to extend the analysis of Zhang *et al.*,<sup>29</sup> limited to straight channels, to investigate the effect of wall curvature on the overshoot effect. The effect of the sinusoidal wall on the temporal evolution of the effective dispersion coefficient is two-fold:

- (c) it induces large oscillations on short/intermediate time scales, especially for large  $\lambda$ , due to the continuous widening and narrowing of the cross section. The peaks of the effective velocity and effective dispersion coefficient occur when the particle swarm passes through the section where the sinusoidal channel has maximum narrowing. The peaks are particularly visible at short time scales when the particle swarm is still compact and has not yet been affected much by the dispersion process. In fact, the first peaks correspond to instants of dimensionless time  $\tau_1 \simeq 3/4\lambda$ ,  $\tau_2 \simeq 7/4\lambda$ , and so on. Correspondingly, the minima are at time instants  $\tau_1 \simeq 1/4\lambda$ ,  $\tau_2 \simeq 5/4\lambda$  when the particle swarm passes through the section where the sinusoidal channel has maximum widening.

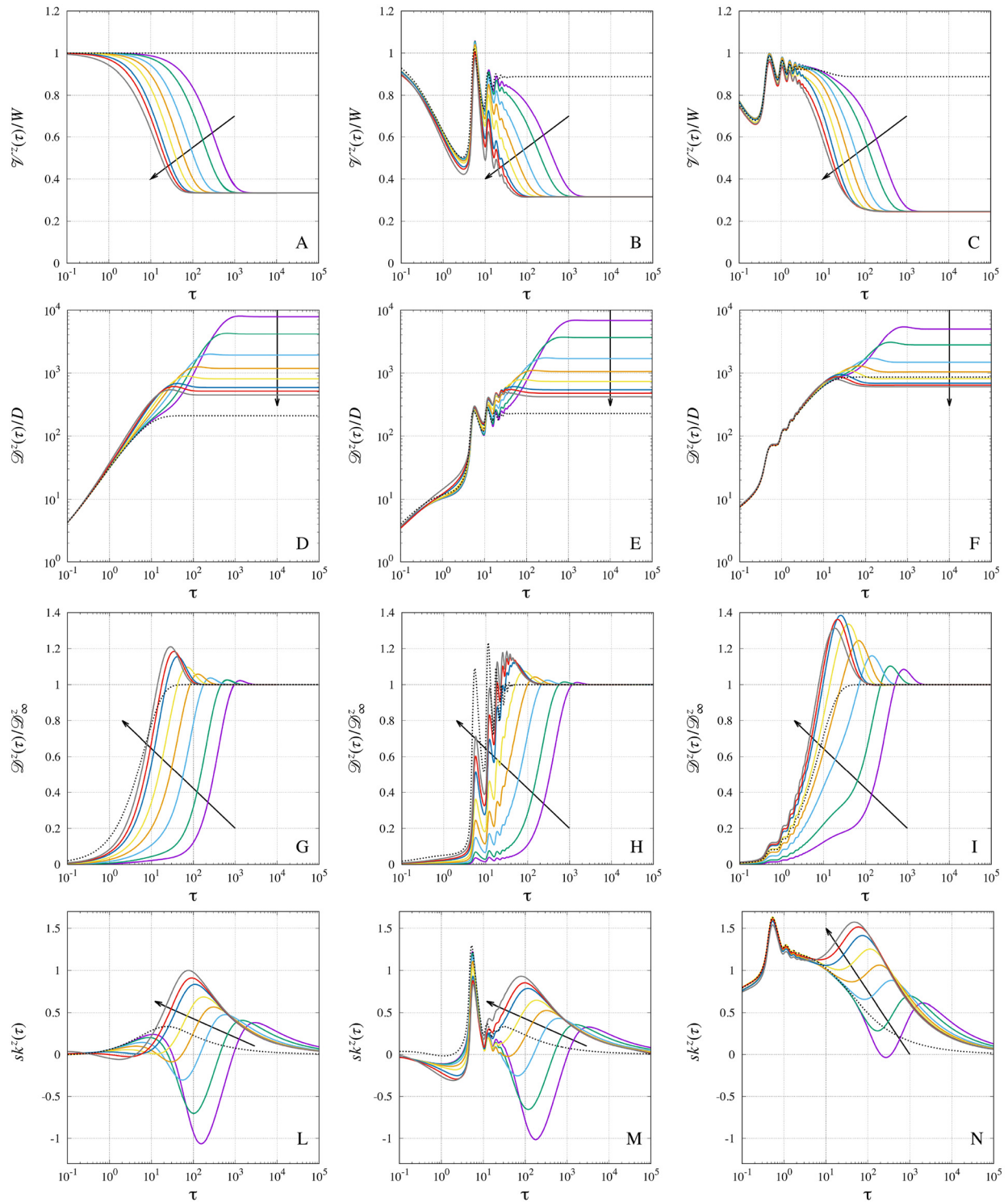


**FIG. 6.** Effective normalized axial velocity  $\mathcal{V}^z(\tau)/W$ , normalized dispersion coefficient  $\mathcal{D}^z(\tau)/D$ , rescaled dispersion coefficient  $\mathcal{D}^z(\tau)/\mathcal{D}_\infty^z$  and skewness  $sk^z(\tau)$  vs  $\tau = tW/R_0$  for a straight tube [panels (a), (d), (g), and (l)], a sinusoidal channel with  $\delta = 0.5$  and  $\lambda = 10$  [panels (b), (e), (h), and (m)] and a sinusoidal channel with  $\delta = 0.5$  and  $\lambda = 2$  [panels (c), (f), (i), and (n)]. Different curves correspond to different values of  $Da_d = 0.1, 0.2, 0.5, 1, 2, 5, 10,$  and  $100$  for  $\gamma = Da_a/Da_d = 1$  and  $Pe = 100$ . Arrows indicate increasing values of  $Da_d$ . Dotted curves represent the behavior in the non-adsorbing case,  $\gamma = 0$ .

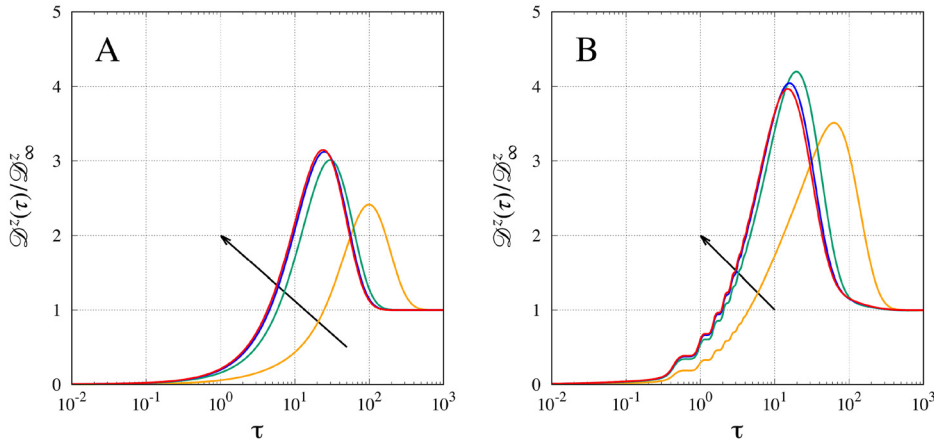


**FIG. 7.** Transient behavior of the rescaled dispersion coefficient  $\mathcal{D}^z(\tau)/\mathcal{D}^z_\infty$  for  $Pe=100$ ,  $\gamma=5$  and different values of  $Da_d = 0.2, 2, 10$ , and  $100$  in the straight tube [panel (a)] and the sinusoidal channel with  $\lambda = 2$  [panel (b)].

- (d) it further amplifies the overshoot effect, with respect to the straight channel, especially for sinusoidal channels with small  $\lambda$ , characterized by the presence of a large recirculation zone for the velocity field. The overshoot effect is further amplified when higher retention factors are considered, as shown in Fig. 7 representing the transient behavior of the rescaled dispersion coefficient  $\mathcal{D}^z(\tau)/\mathcal{D}^z_\infty$  for  $\gamma=5$  and different values of  $Da_d$  in the straight tube and the sinusoidal channel with  $\lambda = 2$ .
5. The adsorption/desorption process strongly affects the temporal evolution of the skewness  $sk^z(\tau)$ , shifting the curves toward high positive values for a fast adsorption/desorption process

( $Da_d > 1$ ) and to negative values for  $Da_d < 1$  when the adsorption/desorption process is the slow/controlling step. This feature can be readily appreciated by comparing the curves  $sk^z(\tau)$  shown in Figs. 6(l)–6(n) with the corresponding ones in the absence of adsorption on tube walls,  $\gamma = 0$ . Large positive or negative values for  $sk^z$  at intermediate time scales  $\tau \approx 10^2$  are associated with a bimodal shape of the marginal distribution  $F_z$  that recovers a unimodal behavior only when the asymptotic behavior  $sk^z(\tau) \sim \tau^{-1/2}$  sets in, as confirmed by the analysis of the marginal pdfs shown in Fig. 8. Figure 8 shows the marginal pdf  $F_z$  at time  $\tau = 100$  for the total

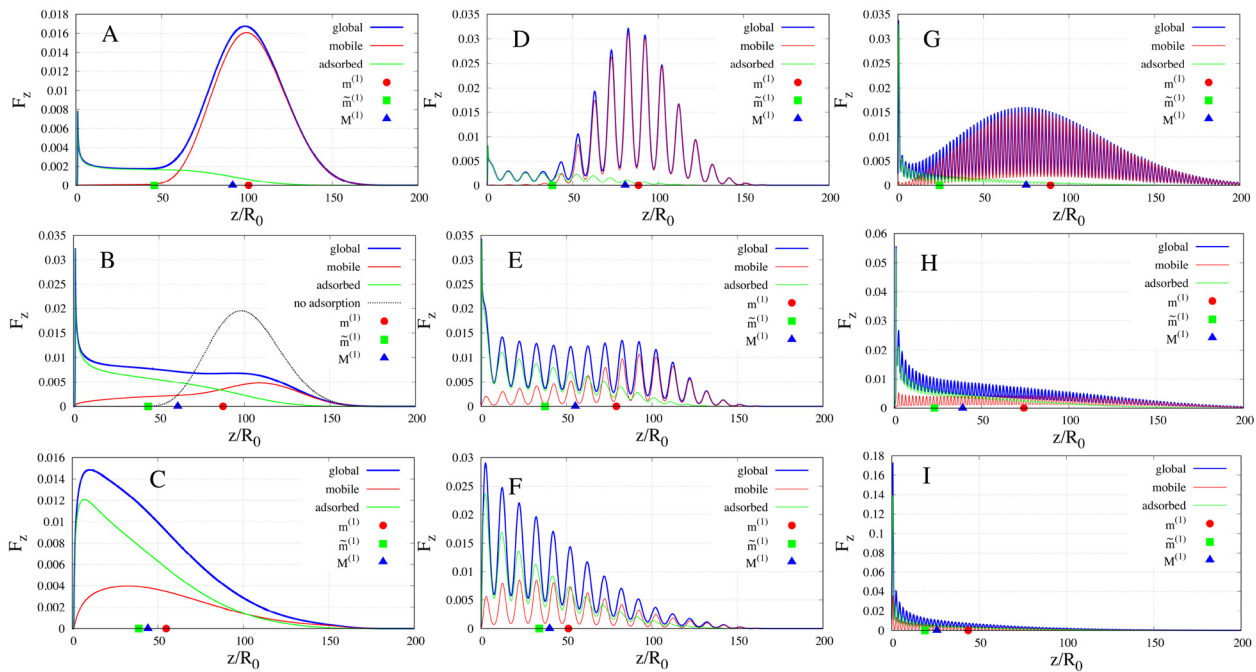


**FIG. 8.** Global marginal distribution  $F_z(z, \tau)$  and weighted marginal distributions  $f_z(z, t) m^{(0)}$  and  $\tilde{f}_z(z, t) \tilde{m}^{(0)}$  in the mobile and adsorbed phase for  $\tau = tW/R_0 = 10^2$ ,  $Pe = 100$ ,  $\gamma = 1$ , and  $Da_a = Da_d = 0.1, 1$ , and  $10$ . Panels (a)–(c) straight tube; Panels (d)–(f) sinusoidal tube with  $\lambda = 10$ . Panels (g)–(i) sinusoidal tube with  $\lambda = 2$ .

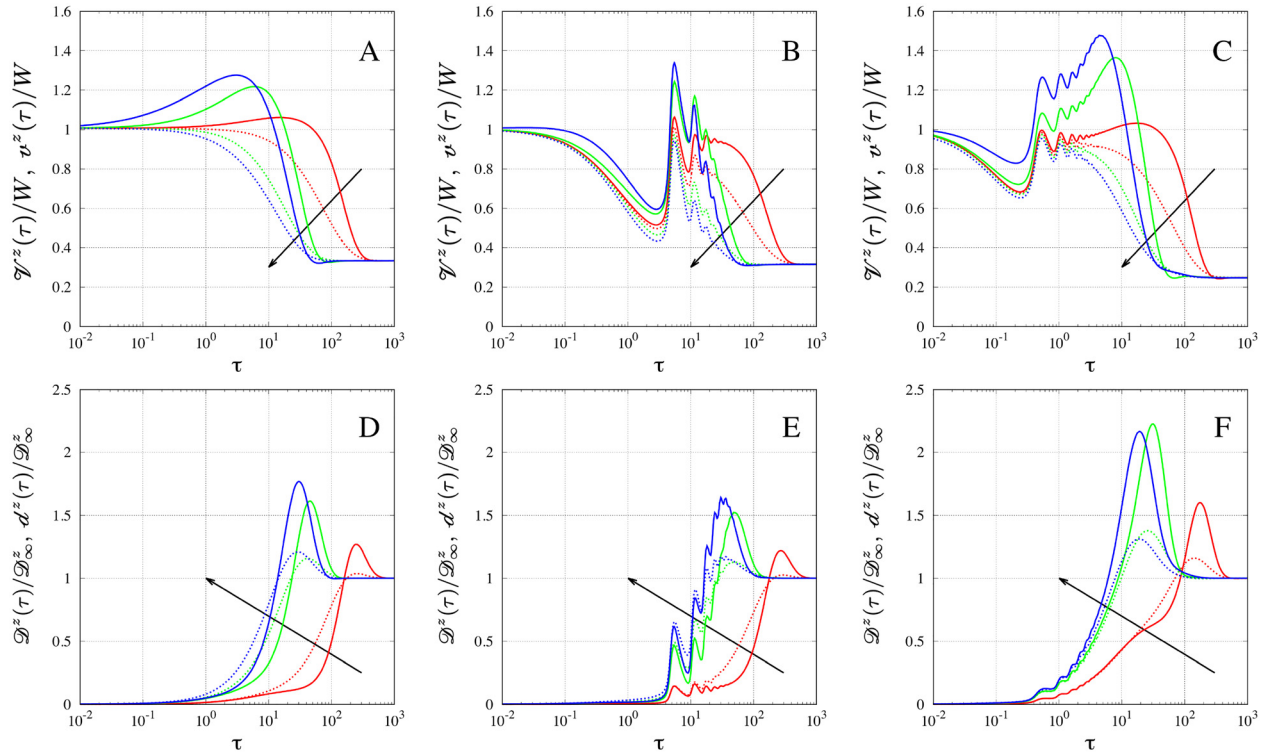


**FIG. 9.** Transient behavior of the normalized velocities  $\mathcal{V}^z(\tau)/W$ ,  $v^z(\tau)/W$  [panels (a)–(c)] and of the rescaled dispersion coefficients  $\mathcal{D}^z(\tau)/\mathcal{D}_\infty^z$ ,  $d^z(\tau)/\mathcal{D}_\infty^z$  [panels (d)–(f)] for  $Pe = 100$ ,  $\gamma = 1$  and different values of  $Da_d = 0.5, 5$ , and  $50$  for the straight tube [panels (a) and (d)] and for the sinusoidal channel with  $\lambda = 10$  [panels (b) and (e)] and  $\lambda = 2$  [panels (c) and (f)]. Continuous lines refer to  $v^z(\tau)/W$  and  $d^z(\tau)/\mathcal{D}_\infty^z$  in the mobile phase, while dashed lines are the corresponding quantities  $\mathcal{V}^z(\tau)/W$  and  $\mathcal{D}^z(\tau)/\mathcal{D}_\infty^z$  for the total solute distribution. Arrows indicate increasing values of  $Da_d$ .

solute distribution, resulting from the convex combination of the two single-phase distributions  $f_z(z, t)$  and  $\tilde{f}_z(z, t)$  in the mobile and adsorbed phase,

$$F_z(z, t) = f_z(z, t) m^{(0)} + \tilde{f}_z(z, t) \tilde{m}^{(0)}, \quad (95)$$

as discussed in Sec. II B. Focusing on the case of a straight channel, Figs. 8(a) and 8(b) show that for  $Da_d = 0.1, 1$  the marginal pdf  $F_z$  is bimodal with a first well pronounced peak due to the particles in the adsorbed phase and a second peak (less pronounced for  $Da_d = 1$ ) due to solute particles in the mobile phase. A long left-side tail can be observed for  $Da_d = 0.1$  [Fig. 8(a)] corresponding to a large negative skewness,  $sk^z \simeq -1$ . For  $Da_d = 1$ , a bimodal/flat distribution can be observed, very different from a Gaussian distribution, even if it possesses a small positive value of the skewness,  $sk^z \simeq 0.2$  almost coinciding with that of the nearly Gaussian total solute distribution in the absence of adsorption [shown as a dotted curve in Fig. 8(b)].

The bimodal shape is intrinsically due to the fact that particles in the mobile and adsorbed phase are traveling at two very different effective velocities, as can be appreciated from the position of the respective first order moments  $m^{(1)}$  and  $\tilde{m}^{(1)}$ , the convex combination of which is the first order moment  $M^{(1)}$ , i.e., the position of the center of mass of the total solute distribution. On the contrary, for  $Da_d = 10$  at the same time  $\tau = 100$ ,

the pdfs  $f_z$  and  $\tilde{f}_z$  overlap and the total pdf  $F_z$  is unimodal although strongly asymmetrical as confirmed by the large positive value of the skewness,  $sk^z \simeq 0.9$ . The dispersion process needs two further decades in time to arrive at a marginal distribution  $F_z$  of Gaussian type during which the skewness can decay to zero as  $\tau^{-1/2}$ . A very similar behavior is observed for the sinusoidal channel with  $\lambda = 10$  [Figs. 8(d)–8(f)] where the wavy shape of the channel wall induces significant oscillations in the marginal pdf  $F_z$  without altering the general trend of the curves. For  $\lambda = 2$ , the effect of the sinusoidal wall is to shorten the left-side tail for  $Da_d = 0.1, 1$  due to the effect of the recirculation zone for a slow adsorption/desorption process. For fast adsorption/desorption ( $Da_d = 10$ ), the marginal pdf  $F_z$  at  $\tau = 100$ , however highly oscillating, is unimodal as in the previous two cases.

The effect of adsorption on the dispersion process can be further analyzed and understood by observing that, at short-intermediate time scales, the effective velocity of the mobile phase  $v^z(\tau)$  is significantly larger than the effective velocity  $\mathcal{V}^z(\tau)$  of the total solute distribution, as shown in Fig. 9. The faster the adsorption/desorption process, the higher the peak for the velocity  $v^z$  in the mobile phase, as expected due to the fast removal of solute particles in the slow-moving region near the tube walls. The effect of the increased velocity on the dispersion coefficient  $d^z(\tau)$  in the mobile phase is compensated by the removal of



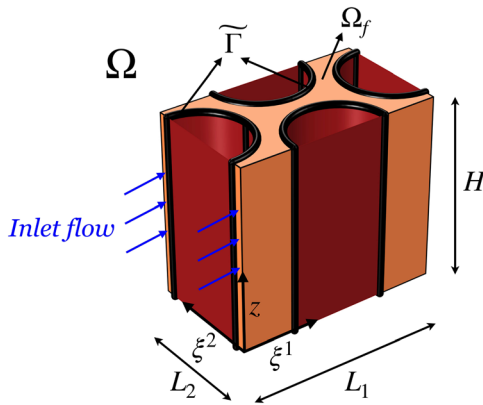


**FIG. 10.** 3D periodic unit cell  $\Omega$  of the retentive pillar array column. The orange region is the fluid domain  $\Omega_f$ , volume  $V_f$ . Red cylinders represent the retentive pillars with diameter  $d$ . Black thick curves highlight the adsorbing/desorbing surface  $\bar{\Gamma}$ .  $L_1/L_2 = \sqrt{3}$ ,  $H = 1.9d$ ,  $\bar{S}/V_f \simeq 5.89$ , Porosity  $V_f/(L_1 \times L_2 \times H) \simeq 0.4$ . The entire structure is obtained by the periodic repetition of the unit cell along the local coordinates  $\xi_1$  and  $\xi_2$ . Top and bottom impermeable walls are placed at  $z = H, 0$ .

solute particles in the wall region where the velocity gradients are larger. For this reason, the dispersion coefficient  $d^z(\tau)$  in the mobile phase is smaller than the dispersion coefficient  $\mathcal{D}^z(\tau)$  of the total solute distribution at short time scales, and specifically before the peak (overshoot effect). In point of fact, the analysis of the transient behavior of  $d^z(\tau)$  shows that the overshoot effect is actually due to a peak in the dispersivity of the mobile phase that disappears when dynamic equilibrium conditions are reached and the fractions  $m^{(0)}$  and  $\tilde{m}^{(0)}$  of solute particles in the mobile and adsorbed phase become constant and equal to  $\lim_{t \rightarrow \infty} m^{(0)} = c_0 = (1 + K)^{-1}$ ,  $\lim_{t \rightarrow \infty} \tilde{m}^{(0)} = \tilde{c}_0 = K(1 + K)^{-1}$ , respectively.

**V. CASE STUDY II: RETENTIVE PILLAR ARRAY COLUMNS FOR LIQUID CHROMATOGRAPHY**

This section analyzes the temporal evolution of dispersion properties of a single solute, driven by a pressure gradient along the  $x^1$  coordinate, in a 3D conduit with rectangular cross section (height  $H = 19$  and width  $500 \mu\text{m}$ ) filled with an array of retentive pillars

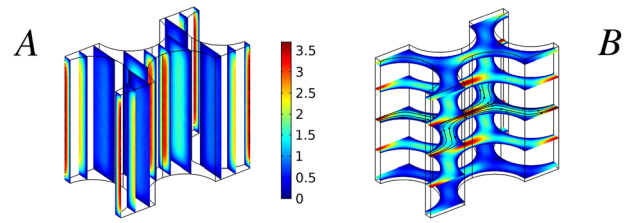


**FIG. 11.** Normalized axial component  $v^1/W$  of the fluid velocity field,  $W$  being the seepage velocity along  $\xi^1$ . Panel (a) view on different  $(\xi^2, z)$  planes; panel (b) view on different  $(\xi^1, \xi^2)$  planes and streamlines on the 2D periodic unit cell adopted for the 2D problem.

(diameter  $d = 10$  and height  $H = 19 \mu\text{m}$ ) arranged on an equilateral triangular grid with sides selected such that the array possesses an external porosity of 40%. This chromatographic column has been experimentally realized by De Malsche *et al.*<sup>18</sup> and the retention factor was estimated as  $K = 0.25$ . The same device was investigated by Yan *et al.*<sup>30</sup> in order to estimate the asymptotic dispersion tensor  $\mathcal{D}^{i,j}_\infty$  under the hypothesis of an instantaneous equilibrium between mobile and adsorbed phase, i.e.,  $Da_d \rightarrow \infty$ .

Here, we investigate the transient and asymptotic behavior of the effective dispersion properties  $\mathcal{V}^1$  and  $\mathcal{D}^{1,1}$  in a wide range of  $Da_d$  by solving the transport equations for the hierarchy of local moments defined on the periodic cell represented in Fig. 10. The transport problem is solved with the assumptions of a constant solute diffusivity  $D$  in the mobile phase and no diffusion on the adsorbing layer. Two cases are considered: (1) a 2D problem that overlooks the effect of the top and bottom non adsorbing walls,  $z = H, 0$ ; (2) a fully 3D problem accounting for the presence of the top and bottom walls where no-slip boundary conditions apply for the velocity field and no-flux boundary conditions are enforced for the local moments. In both cases, the inlet condition is an impulsive injection of solute uniformly distributed over the inlet cross section.

Figures 11(a) and 11(b) show the normalized axial component  $v^1/W$  of the fluid velocity field,  $W$  being the reference velocity chosen as the seepage velocity along  $\xi^1$ , i.e.,  $W = (\int_{\Omega_f} v^1(\xi, z) d\xi dz) / V_f$ , and  $V_f$  the volume of the fluid domain  $\Omega_f$ . Figure 11(b) also highlights the streamlines on the 2D unit cell adopted for the 2D analysis of dispersion features.

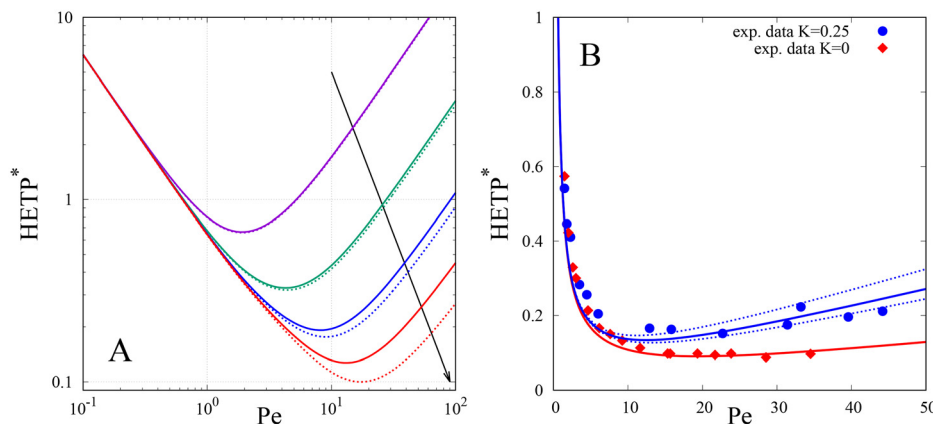


**FIG. 12.** Panel (a) Van Deemter plot  $HETP^* = \mathcal{D}^{(1,1)}_\infty / (\mathcal{V}^1_\infty d)$  vs  $Pe = Wd/D$  for  $K = 0.25$  and  $Da_d = 1, 5, 20$ , and  $100$ . Continuous lines refer to 3D results. Dashed lines indicate 2D results. The arrow indicates increasing values of  $Da_d$ . Panel (b) Experimental data for  $HETP^*$  vs  $Pe$  from Ref. 32 and comparison with 3D theoretical predictions for  $K = 0.25$  and  $Da_d = 75 \pm 25$  (blue curves) and  $K = 0$  (no adsorption, red curve).

Focusing first on the asymptotic behavior, Fig. 12(a) shows the Van Deemter curves for  $K=0.25$  and different values of  $Da_d = 1, 5, 20, 50,$  and  $100$  as obtained from the solution of the transport problem in the 2D and in the 3D periodic cells. As expected, the fully 3D problem furnishes higher values of the dispersion entry  $\mathcal{D}_\infty^{1,1}$  and therefore of the  $HETP^* = \mathcal{D}^{(1,1)}/(\mathcal{V}_\infty^1 d)$  because it accounts for the axial velocity gradients at the top and bottom wall (absent in the 2D formulation of the problem) enhancing the dispersion process. This result is in perfect agreement with the analysis of De Smet *et al.*<sup>85</sup> that observed that, for a similar device, the bottom and top walls contribute

significantly to band broadening. Differences between the 2D and the 3D problem are more pronounced for higher values of  $Da_d$  and this would imply an overestimate of  $Da_d$  in the case of the 2D model is adopted to analyze experimental data. Figure 12(b) shows the good agreement between experimental data for the  $HETP^*$  vs  $Pe$  taken from<sup>18</sup> and 3D model predictions in both the non-adsorbing case  $K=0$  (no fitting parameters) and the adsorbing case with  $K=0.25$  and an estimated optimal value of  $Da_d = 75 \pm 25$  corresponding to an almost instantaneous equilibrium condition between the mobile and adsorbed phase.

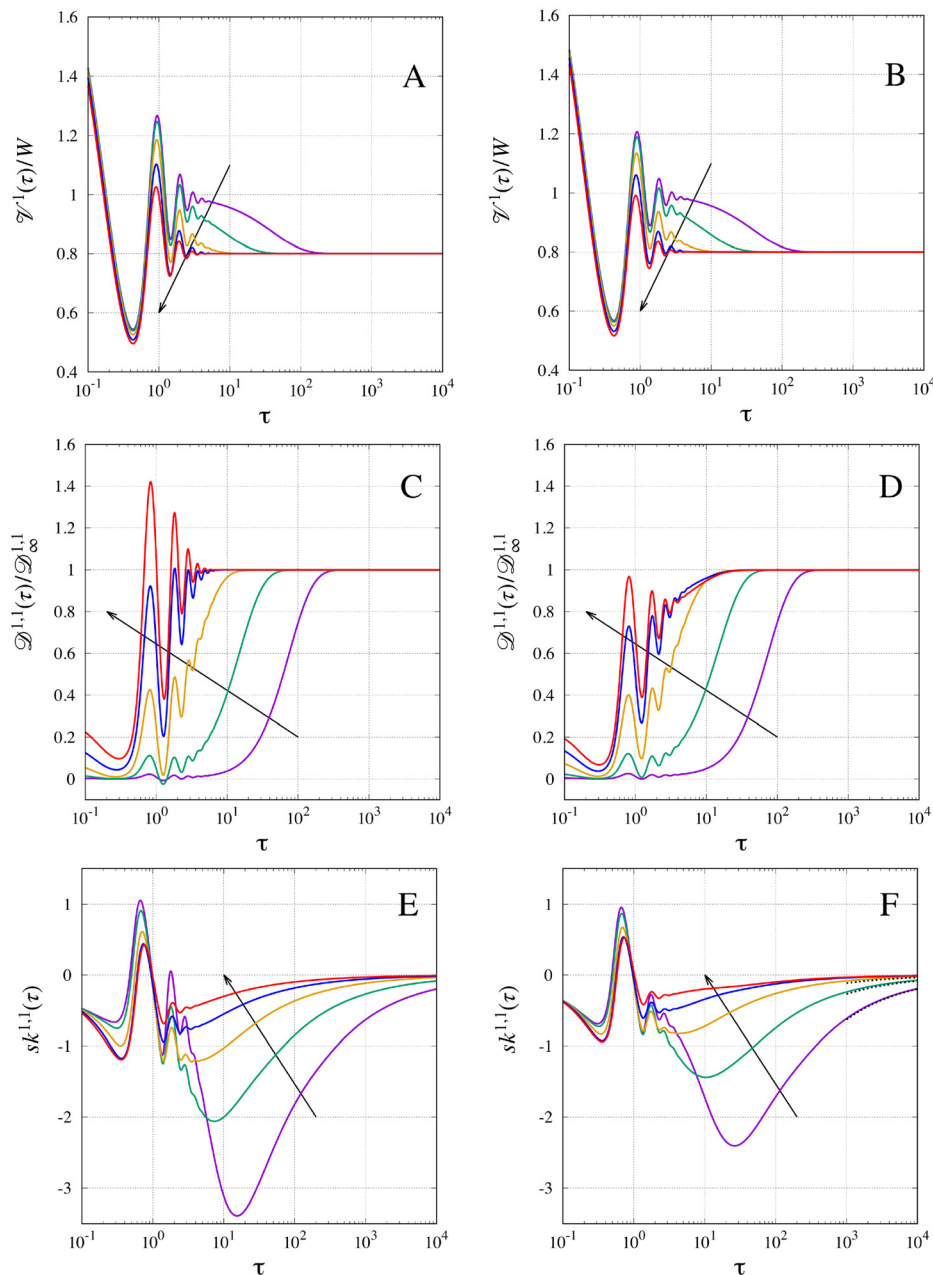


**FIG. 13.** Effective normalized axial velocity  $\mathcal{V}^{1,1}(\tau)/W$ , rescaled axial dispersion coefficient  $\mathcal{D}^{1,1}(\tau)/\mathcal{D}_\infty^{1,1}$  and skewness  $sk^{1,1}(\tau)$  vs  $\tau = tW/d$  for the 2D problem [panels (a), (c), and (e)] and the 3D problem [panels (b), (d), and (f)]. Different curves correspond to  $K=0.25$ ,  $Pe=50$  and different values of  $Da_d = 1, 5, 20, 50,$  and  $100$ . Arrows indicate increasing values of  $Da_d$ . Dashed curves in panel F are the long time scale behavior of the 2D problem, reported for direct comparison with 3D results.

The analysis on the 2D and the 3D unit cells furnishes different results also as it regards the transient behavior of dispersion process, as shown in Figs. 13(a)–13(f). The presence of the pillars induces a tortuous fluid motion which causes oscillations in the temporal evolution of both the effective axial velocity  $\mathcal{V}^1(\tau)$  and the axial dispersion coefficient  $\mathcal{D}^{(1,1)}(\tau)$  similar to that observed in the sinusoidal channel. Oscillations are more damped in the 3D case. As in the sinusoidal channel, the skewness of the marginal distribution  $F_1(x^1, t)$  converges toward 0 slower than  $\mathcal{V}^1(\tau)$  and  $\mathcal{D}^{(1,1)}(\tau)$  converge toward their asymptotic values. However, the convergence toward a Gaussian marginal distribution is significantly faster than in the sinusoidal channel especially for large  $Da_d$  values corresponding to a diffusion-controlled process. The skewness is overestimated in the 2D analysis on short/intermediate time scales but the asymptotic behavior almost coincides in the 2D and the 3D analyses. Unlike what is seen in the sinusoidal channels, the skewness converges to zero from negative values, which implies a left-side persisting tail of the marginal distribution.

## VI. CONCLUSIONS

The homogenization method here proposed represents a robust and computationally efficient continuous approach to investigate the temporal evolution of effective dispersion properties in periodic media with adsorbing/desorbing walls.

The method is based on the introduction of exact local and integral moments. No assumptions must be made on the nature of the velocity field, apart from a sufficient regularity and periodicity on the unit-cell.

The estimate of the transient behavior of the effective velocity vector and the effective dispersion tensor requires exclusively the solution of the time-dependent advection-diffusion equations for the zero-order and first-order exact local moments, defined on the unit-cell. This implies an enormous reduction of the computational efforts and a significant improvement of the accuracy of the results when compared to direct numerical simulation (DNS) approaches that require the solution of the advection-diffusion equation for the analyte concentration in the entire fluid domain. Indeed, if the entire device consists of the periodic repetition of  $N$  identical periodic cells, the computational cost of the DNS approach is equal to  $N/2$  of the computational cost of the moment-based approach. In the case of the retentive pillar array column, the number  $N$  of periodic cells is order of  $10^5$ .

The dynamics of third-order exact moments allows an accurate estimate of the temporal evolution of the asymmetry of the marginal distribution of the analyte along the main flow direction. This permits to correctly identify the time and length scales characterizing the achievement of the macro-transport conditions.

As a first case study, the exact moment method is applied to analyze transient dispersion properties of point-sized particles in sinusoidal tubes, under the action of a pressure-driven Stokes flow. Numerical results are in excellent agreement with stochastic dynamic simulations in a wide range of Peclet values.

A very rich dynamic behavior, characterized by wide and persistent temporal oscillation, is observed for both the effective axial velocity and the axial dispersion coefficient in both microfluidic systems analyzed, namely the sinusoidal channel and the chromatographic column with retentive pillars. The global effect of the retentive walls is (i) to amplify the overshoot effect of the axial dispersion, characterizing

the pre-asymptotic regime, and (II) to slow down the relaxation of the skewness of the marginal distribution toward zero, implying a slower convergence toward a Gaussian distribution characterizing the settling of the macrotransport regime. From a practical point of view, it is important to take into account the temporal fluctuations and the overshoot effect of the effective dispersion coefficient for accurate estimation of the minimum device length that will ensure that macrotransport conditions are achieved.

One possible and straightforward application of the exact moment method is the transient and asymptotic analysis of mass transport in streaming blood (pulsatile or steady conditions) through a stenotic artery with mass transfer at the rigid boundary. This interesting problem will certainly be the subject of future investigation.

## AUTHOR DECLARATIONS

### Conflict of Interest

The authors have no conflicts to disclose.

### Author Contributions

**Claudia Venditti:** Conceptualization (equal); Data curation (equal); Formal analysis (equal); Investigation (equal); Methodology (equal); Software (equal); Writing – review & editing (equal). **Massimiliano Giona:** Conceptualization (equal); Methodology (equal); Supervision (equal). **Alessandra Adrover:** Conceptualization (equal); Data curation (equal); Formal analysis (equal); Investigation (equal); Methodology (equal); Software (equal); Supervision (equal); Writing – original draft (equal); Writing – review & editing (equal).

## DATA AVAILABILITY

The data that support the findings of this study are available from the corresponding author upon reasonable request.

## NOMENCLATURE

$b_{i,j}(\xi), \tilde{b}_{i,j}(\tilde{\xi})$ (m)	b-field in the mobile, adsorbed phase
$c_0, \tilde{c}_0$ (-)	Fraction of solute particles in the mobile, adsorbed phase
$c_{i,j}(\xi), \tilde{c}_{i,j}(\tilde{\xi})$ (m <sup>2</sup> )	c-field in the mobile, adsorbed phase
$\mathbf{D}(\mathbf{x})$ (m <sup>2</sup> /s)	Position-dependent diffusion tensor of the analyte
$Da_a, Da_d$ (-)	Adsorption, desorption Damköhler number
$F_i(x^i, t)$ (1/m)	marginal probability density function
$h_q(t)$	Interaction term for the qth order moment
$H$ (m)	Height of the pillars
$HETP^*$	Dimensionless Height Equivalent of a Theoretical Plate
$\mathbf{J}[\cdot]$	Flux operator
$k_a(\tilde{\mathbf{x}})$ (m/s)	Position-dependent adsorption kinetic constant
$k_d(\tilde{\mathbf{x}})$ (1/s)	Position-dependent desorption kinetic constant
$K$ (-)	Average retention factor
$L$ (m)	Wavelength of the sinusoidal channel
$L_i$ (m)	Periodicity length along the unit lattice vector $\mathbf{e}_i$

$m^i$ (-)	Unit cell number along the unit lattice vector $e_i$
$m_{q_1, q_2}^{(q)}(t)$ ( $m^q$ )	qth order integral moments in the mobile phase
$\tilde{m}_{q_1, q_2}^{(q)}(t)$ ( $m^q$ )	qth order integral moments in the adsorbed phase
$M_{q_1, q_2}^{(q)}(t)$ ( $m^q$ )	qth order integral moment of the total solute distribution
$N_{q_1, q_2}^{(q)}(t)$ ( $m^q$ )	Integral moment defined according to Brenner's approach
$p(\mathbf{x}, t)$ ( $1/m^3$ )	Normalized analyte concentration in the mobile phase
$\tilde{p}(\tilde{\mathbf{x}}, t)$ ( $1/m^2$ )	Normalized analyte concentration in the adsorbed phase
$\bar{p}(\mathbf{X}, t)$ ( $1/m^3$ )	Average analyte concentration over the periodicity cell
$P_{q_1, q_2}^{(q)}(\xi, t)$ ( $m^q/m^3$ )	Exact local moments in the mobile phase
$\tilde{P}_{q_1, q_2}^{(q)}(\tilde{\xi}, t)$ ( $m^q/m^2$ )	Exact local moments in the adsorbed phase
$Pe$ (-)	Peclét number
$q_i$ (-)	Order of the moment along the unit lattice vector $e_i$
$Q_{q_1, q_2}^{(q)}(\xi, t)$ ( $m^q/m^3$ )	Quantized local moments in the mobile phase
$\tilde{Q}_{q_1, q_2}^{(q)}(\tilde{\xi}, t)$ ( $m^q/m^2$ )	Quantized local moments in the adsorbed phase
$R_0$ (m)	Average radius of the sinusoidal channel
$sk^{(i,j)}(t)$ (-)	Time-dependent skewness
$\tilde{S}$ ( $m^2$ )/(m)	Area/length of the adsorbing boundary
$\mathbf{v}(\mathbf{x})$ (m/s)	Eluent velocity field
$V_f$ ( $m^3$ )/( $m^2$ )	Volume/area) of the fluid phase
$w_0(\xi)$ ( $1/m^2$ )	Frobenius eigenfunction of the Laplacian operator in the mobile phase
$\tilde{w}_0(\tilde{\xi})$ ( $1/m^2$ )	Counterpart of $w_0(\xi)$ in the adsorbed phase
$W$ (m/s)	Average axial velocity at the inlet section of the unit cell of the sinusoidal channel
$\mathbf{x}, \tilde{\mathbf{x}}$	Any point in the mobile, adsorbed phase
$\bar{\mathbf{x}}$	Any point on the non-adsorbent part of the obstacle surface
$\mathbf{X}$	Long-range spatial variable

Greek symbols

$\gamma$ (-)	Equilibrium constant
$\Gamma, \tilde{\Gamma}$	Non-adsorbing, adsorbing portion of solid boundary of cell domain
$\Delta, \tilde{\Delta}$	Non-absorbing, absorbing portion of solid boundary of the domain
$\delta$ (-)	Dimensionless wave amplitude of the sinusoidal channel
$\zeta$	Local coordinate in the sinusoidal channel
$\lambda$ (-)	Dimensionless wavelength of the sinusoidal channel
$\mu_{i,j}^{(3)}$ ( $m^3$ )	Centered third-order moments of the global solute distribution
$\xi, \tilde{\xi}$	Local coordinates in the mobile, adsorbed phase
$\Sigma_f$	Fluid domain
$\Sigma_s$	Solid domain
$\sigma_{i,j}^2$ ( $m^2$ )	Variances of the global solute distribution
$\tau$	Dimensionless time

$\chi, \tilde{\chi}$	Local coordinates in the sinusoidal channel in the mobile, adsorbed phase
$\Omega$	Cell domain
$\Omega_f$	Fluid cell domain

Calligraphic symbols

$d^{i,j}, \tilde{d}^{i,j}$ ( $m^2/s$ )	Effective dispersion tensor in the mobile, adsorbed phase
$d_{\infty}^{i,j}, \tilde{d}_{\infty}^{i,j}$ ( $m^2/s$ )	Asymptotic effective dispersion tensor in the mobile, adsorbed phase
$\mathcal{D}^{i,j}$ ( $m^2/s$ )	Entries of the effective symmetric dispersion tensor
$\mathcal{D}_{\infty}^{i,j}$ ( $m^2/s$ )	Entries of the asymptotic effective symmetric dispersion tensor
$\mathcal{L}_{\xi}[\cdot]$	Cell advection-diffusion operator
$\mathcal{L}_{\zeta,r}[\cdot]$	Cell advection-diffusion operator in cylindrical coordinates
$s_{i,j}^2, \tilde{s}_{i,j}^2$ ( $m^2$ )	Variances of the particle density functions in the mobile, adsorbed phase
$v^i, \tilde{v}^i$ (m/s)	Velocity component of solute particles in the mobile, adsorbed phase
$v_{\infty}^i, \tilde{v}_{\infty}^i$ (m/s)	Asymptotic velocity component of solute particles in the mobile, adsorbed phase
$\mathcal{V}^i$ (m/s)	Entries of the effective velocity field
$\mathcal{V}_{\infty}^i$ (m/s)	Entries of the asymptotic effective velocity field

APPENDIX: NUMERICAL ISSUE

Numerical results for the stationary velocity field and for the space-time evolution of local moments in 2D and 3D geometries were obtained by solving the corresponding partial differential equations with a commercial software enforcing finite-element method (Comsol 5.5).

For the velocity field, the incompressible Navier–Stokes package (Stokes flow) in stationary conditions was adopted with P2+P1 Lagrange elements (velocity+pressure).

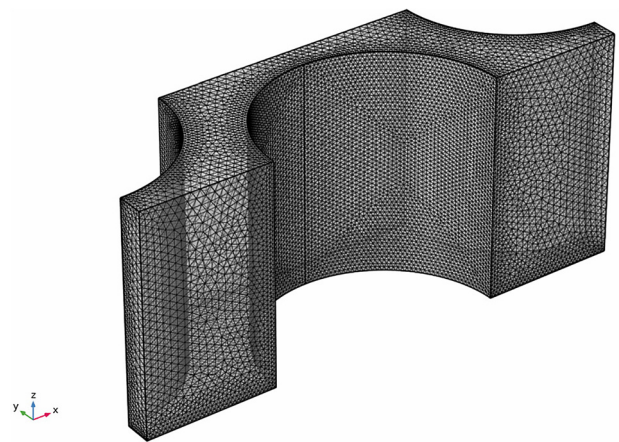


FIG. 14. Mesh adopted for the 3D problem. The velocity field and the transport problems for  $P_{q_1, q_2}^{(q)}$  and  $\tilde{P}_{q_1, q_2}^{(q)}$  were solved on a smaller portion of the domain (1/4) by enforcing the symmetry conditions along both the vertical z axis and the horizontal y axis.

For the numerical integration of the coupled transport equations for  $P_{q1,q2}^{(q)}$  and  $\tilde{P}_{q1,q2}^{(q)}$  Eqs. (18)–(23), the coefficient form PDE and the boundary ODEs packages were adopted and solved in transient conditions (time-dependent segregated approach). Lagrangian quadratic elements have been chosen. MUMPS linear solver was adopted with relative tolerance  $10^{-3}$  and absolute tolerance  $10^{-6}$ . The number of finite triangular elements for the 2D axial-symmetric sinusoidal channel was order of  $2 \times 10^5$  with a non-uniform mesh. Smaller elements were located at the sinusoidal boundary (maximum element size  $2 \times 10^{-3}$ ) and at the periodic boundaries  $\zeta = 0, \lambda$  (maximum element size  $1 \times 10^{-3}$ ). For the 3D microchannel, numerical results in stationary and transient conditions were obtained on a tetrahedral mesh consisting of  $6 \times 10^5$  domain elements, about  $4 \times 10^4$  boundary elements, and  $1 \times 10^3$  edge elements (see Fig. 14). The meshes adopted guarantee that the numerical results obtained are mesh independent for all the values of  $Pe$  investigated, namely  $Pe \in (10^{-1}, 10^3)$ .

## REFERENCES

- <sup>1</sup>A. Adrover, S. Cerbelli, F. Garofalo, and M. Giona, “Convection-dominated dispersion regime in wide-bore chromatography: A transport-based approach to assess the occurrence of slip flows in microchannels,” *Anal. Chem.* **81**, 8009–8014 (2009).
- <sup>2</sup>A. Ajdari, N. Bontoux, and H. A. Stone, “Hydrodynamic dispersion in shallow microchannels: The effect of cross-sectional shape,” *Anal. Chem.* **78**, 387–392 (2006).
- <sup>3</sup>T. Motz, G. Schmid, P. Hänggi, D. Reguera, and J. M. Rubí, “Optimizing the performance of the entropic splitter for particle separation,” *J. Chem. Phys.* **141**, 074104 (2014).
- <sup>4</sup>C.-O. Ng and Q. Zhou, “Dispersion due to electroosmotic flow in a circular microchannel with slowly varying wall potential and hydrodynamic slippage,” *Phys. Fluids* **24**, 112002 (2012).
- <sup>5</sup>C. Vargas, J. Arcos, O. Bautista, and F. Mendez, “Hydrodynamic dispersion in a combined magnetohydrodynamic-electroosmotic-driven flow through a microchannel with slowly varying wall zeta potentials,” *Phys. Fluids* **29**, 092002 (2017).
- <sup>6</sup>B. Ling, M. Oostrom, A. M. Tartakovsky, and I. Battiato, “Hydrodynamic dispersion in thin channels with micro-structured porous walls,” *Phys. Fluids* **30**, 076601 (2018).
- <sup>7</sup>Z. Wu and N.-T. Nguyen, “Convective–diffusive transport in parallel lamination micromixers,” *Microfluid. Nanofluid.* **1**, 208–217 (2005).
- <sup>8</sup>N.-T. Nguyen, “Mixing in microscale,” in *Microfluidic Technologies for Miniaturized Analysis Systems*, edited by S. Hardt and F. Schönfeld (Springer US, Boston, MA, 2007), pp. 117–155.
- <sup>9</sup>F. Garofalo, A. Adrover, S. Cerbelli, and M. Giona, “Spectral characterization of static mixers. The S-shaped micromixer as a case study,” *AIChE J.* **56**, 318–335 (2009).
- <sup>10</sup>V. Biagioni, A. L. Sow, A. Adrover, and S. Cerbelli, “Brownian sieving effect for boosting the performance of microcapillary hydrodynamic chromatography. proof of concept,” *Anal. Chem.* **93**, 6808–6816 (2021).
- <sup>11</sup>V. Biagioni, A. L. Sow, A. G. Fagiolo, A. Adrover, and S. Cerbelli, “Brownian sieving enhancement of microcapillary hydrodynamic chromatography. Analysis of the separation performance based on Brenner’s macro-transport theory,” *J. Chromatogr. A* **1659**, 462652 (2021).
- <sup>12</sup>C. Venditti, S. Cerbelli, G. Procopio, and A. Adrover, “Comparison between one- and two-way coupling approaches for estimating effective transport properties of suspended particles undergoing Brownian sieving hydrodynamic chromatography,” *Phys. Fluids* **34**, 042010 (2022).
- <sup>13</sup>M. Blom, E. Chmela, J. Gardeniers, R. Tjisse, M. Elwenspoek, and A. van den Berg, “Design and fabrication of a hydrodynamic chromatography chip,” *Sens. Actuators, B* **82**, 111–116 (2002).
- <sup>14</sup>M. Blom, E. Chmela, R. Oosterbroek, R. Tjissen, and A. van den Berg, “On-chip hydrodynamic chromatography separation and detection of nanoparticles and biomolecules,” *Anal. Chem.* **75**, 6761–6768 (2003).
- <sup>15</sup>J. Auriault and P. Adler, “Taylor dispersion in porous media: Analysis by multiple scale expansions,” *Adv. Water Resour.* **18**, 217–226 (1995).
- <sup>16</sup>M. Paine, R. Carbonell, and S. Whitaker, “Dispersion in pulsed systems—I: Heterogenous reaction and reversible adsorption in capillary tubes,” *Chem. Eng. Sci.* **38**, 1781–1793 (1983).
- <sup>17</sup>R. Carbonell and S. Whitaker, “Dispersion in pulsed systems—II: Theoretical developments for passive dispersion in porous media,” *Chem. Eng. Sci.* **38**, 1795–1802 (1983).
- <sup>18</sup>W. De Malsche, D. Clicq, V. Verdoold, P. Gzil, G. Desmet, and H. Gardeniers, “Integration of porous layers in ordered pillar arrays for liquid chromatography,” *Lab Chip* **7**, 1705–1711 (2007).
- <sup>19</sup>H. Brenner and D. A. Edwards, *Macrotransport Processes* (Butterworth-Heinemann, 1993).
- <sup>20</sup>H. C. W. Chu, S. Garoff, T. M. Przybycien, R. D. Tilton, and A. S. Khair, “Dispersion in steady and time-oscillatory two-dimensional flows through a parallel-plate channel,” *Phys. Fluids* **31**, 022007 (2019).
- <sup>21</sup>D. L. Koch and J. F. Brady, “A non-local description of advection-diffusion with application to dispersion in porous media,” *J. Fluid Mech.* **180**, 387–403 (1987).
- <sup>22</sup>A. Nadim, “Dispersion in spatially periodic media: The moment-difference expansion method,” *SIAM J. Appl. Math.* **49**, 1524–1537 (1989).
- <sup>23</sup>A. Adrover and S. Cerbelli, “Laminar dispersion at low and high Peclet numbers in finite-length patterned microtubes,” *Phys. Fluids* **29**, 062005 (2017).
- <sup>24</sup>A. Adrover, S. Cerbelli, and M. Giona, “Taming axial dispersion in hydrodynamic chromatography columns through wall patterning,” *Phys. Fluids* **30**, 042002 (2018).
- <sup>25</sup>A. Adrover, C. Passaretti, C. Venditti, and M. Giona, “Exact moment analysis of transient dispersion properties in periodic media,” *Phys. Fluids* **31**, 112002 (2019).
- <sup>26</sup>H. Brenner and K. Stewartson, “Dispersion resulting from flow through spatially periodic porous media,” *Philos. Trans. R. Soc. London, Ser. A* **297**, 81–133 (1980).
- <sup>27</sup>M. Levesque, O. Bénichou, R. Voituriez, and B. Rotenberg, “Taylor dispersion with adsorption and desorption,” *Phys. Rev. E* **86**, 036316 (2012).
- <sup>28</sup>M. Levesque, O. Bénichou, and B. Rotenberg, “Molecular diffusion between walls with adsorption and desorption,” *J. Chem. Phys.* **138**, 034107 (2013).
- <sup>29</sup>L. Zhang, M. A. Hesse, and M. Wang, “Transient solute transport with sorption in Poiseuille flow,” *J. Fluid Mech.* **828**, 733–752 (2017).
- <sup>30</sup>X. Yan, Q. Wang, and H. H. Bau, “Dispersion in retentive pillar array columns,” *J. Chromatogr. A* **1217**, 1332–1342 (2010).
- <sup>31</sup>M. A. Khan, “Non-equilibrium theory of gas-liquid chromatography,” *Nature* **186**, 800–801 (1960).
- <sup>32</sup>D. Dutta, “Band broadening in mobility shift affinity capillary electrophoresis due to pressure-driven flow,” *Phys. Fluids* **33**, 103602 (2021).
- <sup>33</sup>R. Sankarasubramanian, W. N. Gill, and T. B. Benjamin, “Unsteady convective diffusion with interphase mass transfer,” *Proc. R. Soc. London, Ser. A* **333**, 115–132 (1973).
- <sup>34</sup>P. Wang and G. Chen, “Basic characteristics of Taylor dispersion in a laminar tube flow with wall absorption: Exchange rate, advection velocity, dispersivity, skewness and kurtosis in their full time dependence,” *Int. J. Heat Mass Transfer* **109**, 844–852 (2017).
- <sup>35</sup>A. K. Roy and O. A. Bég, “Asymptotic study of unsteady mass transfer through a rigid artery with multiple irregular stenoses,” *Appl. Math. Comput.* **410**, 126485 (2021).
- <sup>36</sup>S. Debmath, W. Jiang, M. Guan, and G. Chen, “Effect of ring-source release on dispersion process in Poiseuille flow with wall absorption,” *Phys. Fluids* **34**, 027106 (2022).
- <sup>37</sup>W. Q. Jiang and G. Q. Chen, “Solution of gill’s generalized dispersion model: Solute transport in Poiseuille flow with wall absorption,” *Int. J. Heat Mass Transfer* **127**, 34–43 (2018).
- <sup>38</sup>R. Mauri, “Dispersion, convection, and reaction in porous media,” *Phys. Fluids A* **3**, 743–756 (1991).
- <sup>39</sup>S. Haber and R. Mauri, “Lagrangian approach to time-dependent laminar dispersion in rectangular conduits. Part 1. Two-dimensional flows,” *J. Fluid Mech.* **190**, 201–215 (1988).
- <sup>40</sup>A. Sarkar and G. Jayaraman, “The effect of wall absorption on dispersion in oscillatory flow in an annulus: Application to a catheterized artery,” *Acta Mech.* **172**, 151–167 (2004).

- <sup>41</sup>C.-O. Ng and N. Rudraiah, "Convective diffusion in steady flow through a tube with a retentive and absorptive wall," *Phys. Fluids* **20**, 073604 (2008).
- <sup>42</sup>S. Datta and S. Ghosal, "Dispersion due to wall interactions in microfluidic separation systems," *Phys. Fluids* **20**, 012103 (2008).
- <sup>43</sup>J. Rana and P. V. S. N. Murthy, "Unsteady solute dispersion in Herschel-Bulkley fluid in a tube with wall absorption," *Phys. Fluids* **28**, 111903 (2016).
- <sup>44</sup>S. Debnath, A. K. Saha, B. S. Mazumder, and A. K. Roy, "Dispersion phenomena of reactive solute in a pulsatile flow of three-layer liquids," *Phys. Fluids* **29**, 097107 (2017).
- <sup>45</sup>A. Alexandre, T. Guérin, and D. S. Dean, "Generalized Taylor dispersion for translationally invariant microfluidic systems," *Phys. Fluids* **33**, 082004 (2021).
- <sup>46</sup>A. Nadim, M. Pagitsas, and H. Brenner, "Higher-order moments in macrotransport processes," *J. Chem. Phys.* **85**, 5238–5245 (1986).
- <sup>47</sup>R. Mauri, "Lagrangian self-diffusion of Brownian particles in periodic flow fields," *Phys. Fluids* **7**, 275–284 (1995).
- <sup>48</sup>M. Latini and A. J. Bernoff, "Transient anomalous diffusion in Poiseuille flow," *J. Fluid Mech.* **441**, 399–411 (2001).
- <sup>49</sup>E. Taghizadeh, F. J. Valdés-Parada, and B. D. Wood, "Preasymptotic Taylor dispersion: Evolution from the initial condition," *J. Fluid Mech.* **889**, A5 (2020).
- <sup>50</sup>R. Mauri and S. Haber, "Time-dependent dispersion of small particles in rectangular conduits," *SIAM J. Appl. Math.* **51**, 1538–1555 (1991).
- <sup>51</sup>R. R. Ratnakar and V. Balakotaiah, "Exact averaging of laminar dispersion," *Phys. Fluids* **23**, 023601 (2011).
- <sup>52</sup>B. Chakrabarti and D. Saintillan, "Shear-induced dispersion in peristaltic flow," *Phys. Fluids* **32**, 113102 (2020).
- <sup>53</sup>S. Dhar, N. Poddar, K. K. Mondal, and B. S. Mazumder, "On dispersion of solute in a hydromagnetic flow between two parallel plates with boundary absorption," *Phys. Fluids* **33**, 083609 (2021).
- <sup>54</sup>M. Sadeghi, M. H. Saidi, A. Moosavi, and A. Sadeghi, "Unsteady solute dispersion by electrokinetic flow in a polyelectrolyte layer-grafted rectangular microchannel with wall absorption," *J. Fluid Mech.* **887**, A13 (2020).
- <sup>55</sup>P. Das, J. R. Sarifuddin, and P. K. Mandal, "Solute dispersion in transient Casson fluid flow through stenotic tube with exchange between phases," *Phys. Fluids* **33**, 061907 (2021).
- <sup>56</sup>A. Berezhkovskii and G. Hummer, "Single-file transport of water molecules through a carbon nanotube," *Phys. Rev. Lett.* **89**, 064503 (2002).
- <sup>57</sup>J. Karger and D. M. Ruthven, *Diffusion in Zeolites and Other Microporous Solids* (Wiley, 1992).
- <sup>58</sup>D. Holcman and Z. Schuss, "Control of flux by narrow passages and hidden targets in cellular biology," *Rep. Prog. Phys.* **76**, 074601 (2013).
- <sup>59</sup>J. H. Forrester and D. F. Young, "Flow through a converging-diverging tube and its implications in occlusive vascular disease—I: Theoretical development," *J. Biomechanics* **3**, 297–305 (1970).
- <sup>60</sup>A. Adrover, C. Venditti, and M. Giona, "Laminar dispersion at low and high Peclet numbers in a sinusoidal microtube: Point-size versus finite-size particles," *Phys. Fluids* **31**, 062003 (2019).
- <sup>61</sup>D. Reguera and J. M. Rubí, "Kinetic equations for diffusion in the presence of entropic barriers," *Phys. Rev. E* **64**, 061106 (2001).
- <sup>62</sup>D. Reguera, G. Schmid, P. S. Burada, J. M. Rubí, P. Reimann, and P. Hänggi, "Entropic transport: Kinetics, scaling, and control mechanisms," *Phys. Rev. Lett.* **96**, 130603 (2006).
- <sup>63</sup>P. Kalinay and J. K. Percus, "Projection of two-dimensional diffusion in a narrow channel onto the longitudinal dimension," *J. Chem. Phys.* **122**, 204701 (2005).
- <sup>64</sup>P. Kalinay and J. K. Percus, "Corrections to the Fick-Jacobs equation," *Phys. Rev. E* **74**, 041203 (2006).
- <sup>65</sup>M. Mangeat, T. Guérin, and D. S. Dean, "Geometry controlled dispersion in periodic corrugated channels," *Europhys. Lett.* **118**, 40004 (2017).
- <sup>66</sup>E. Yariv and K. D. Dorfman, "Electrophoretic transport through channels of periodically varying cross section," *Phys. Fluids* **19**, 037101 (2007).
- <sup>67</sup>K. D. Dorfman, "Combined electrophoretic and electro-osmotic transport through channels of periodically varying cross section," *Phys. Fluids* **20**, 037102 (2008).
- <sup>68</sup>K. D. Dorfman, "Taylor-Aris dispersion during lubrication flow in a periodic channel," *Chem. Eng. Commun.* **197**, 39–50 (2009).
- <sup>69</sup>N. Laachi, M. Kenward, E. Yariv, and K. D. Dorfman, "Force-driven transport through periodic entropy barriers," *Europhys. Lett.* **80**, 50009 (2007).
- <sup>70</sup>D. Bolster, M. Dentz, and T. L. Borgne, "Solute dispersion in channels with periodically varying apertures," *Phys. Fluids* **21**, 056601 (2009).
- <sup>71</sup>S. Martens, G. Schmid, L. Schimansky-Geier, and P. Hänggi, "Biased Brownian motion in extremely corrugated tubes," *Chaos* **21**, 047518 (2011).
- <sup>72</sup>S. Martens, A. V. Straube, G. Schmid, L. Schimansky-Geier, and P. Hänggi, "Hydrodynamically enforced entropic trapping of Brownian particles," *Phys. Rev. Lett.* **110**, 010601 (2013).
- <sup>73</sup>S. Martens, G. Schmid, A. Straube, L. Schimansky-Geier, and P. Hänggi, "How entropy and hydrodynamics cooperate in rectifying particle transport," *Eur. Phys. J. Spec. Top.* **222**, 2453–2463 (2013).
- <sup>74</sup>S. Martens, A. V. Straube, G. Schmid, L. Schimansky-Geier, and P. Hänggi, "Giant enhancement of hydrodynamically enforced entropic trapping in thin channels," *Eur. Phys. J. Spec. Top.* **223**, 3095–3111 (2014).
- <sup>75</sup>P. Margaretti, I. Pagonabarraga, and J. M. Rubí, "Entropic electrokinetics: Recirculation, particle separation, and negative mobility," *Phys. Rev. Lett.* **113**, 128301 (2014).
- <sup>76</sup>S. Vedel, E. Hovad, and H. Bruus, "Time-dependent Taylor-Aris dispersion of an initial point concentration," *J. Fluid Mech.* **752**, 107–122 (2014).
- <sup>77</sup>H. Orihara and Y. Takikawa, "Brownian motion in shear flow: Direct observation of anomalous diffusion," *Phys. Rev. E* **84**, 061120 (2011).
- <sup>78</sup>D. Chakraborty, "Time correlations and persistence probability of a Brownian particle in a shear flow," *Eur. Phys. J. B* **85**, 281 (2012).
- <sup>79</sup>E. O. Fridjonsson, J. D. Seymour, and S. L. Codd, "Anomalous preasymptotic colloid transport by hydrodynamic dispersion in microfluidic capillary flow," *Phys. Rev. E* **90**, 010301 (2014).
- <sup>80</sup>K. D. Dorfman and H. Brenner, "Convective dispersion without molecular diffusion," *Physica A* **322**, 180–194 (2003).
- <sup>81</sup>A. M. Berezhkovskii and A. T. Skvortsov, "Aris-Taylor dispersion with drift and diffusion of particles on the tube wall," *J. Chem. Phys.* **139**, 084101 (2013).
- <sup>82</sup>J. van Deemter, F. Zuiderweg, and A. Klinkenberg, "Longitudinal diffusion and resistance to mass transfer as causes of nonideality in chromatography," *Chem. Eng. Sci.* **5**, 271–289 (1956).
- <sup>83</sup>J. H. Knox, "Band dispersion in chromatography—a universal expression for the contribution from the mobile zone," *J. Chromatogr. A* **960**, 7–18 (2002).
- <sup>84</sup>S. Vedel and H. Bruus, "Transient Taylor-Aris dispersion for time-dependent flows in straight channels," *J. Fluid Mech.* **691**, 95–122 (2012).
- <sup>85</sup>J. D. Smet, P. Gzil, G. Baron, and G. Desmet, "On the 3-dimensional effects in etched chips for high performance liquid chromatography-separations," *J. Chromatogr. A* **1154**, 189–197 (2007).